Mathematical Relationships between Spinal Motoneuron Properties

Arnault Caillet[1], Andrew T.M. Phillips[1], Dario Farina[2,*], Luca Modenese[1,*]

[1]Department of Civil and Environmental Engineering, Imperial College London, SW7 2AZ, UK
[2]Department of Bioengineering, Imperial College London, SW7 2AZ, UK
Email: arnault.caillet17@imperial.ac.uk

* These authors have equal contributions and share the senior authorship

NUMBER OF PAGES: 45

NUMBER OF FIGURES: 7

NUMBER OF TABLES: 8

NUMBER OF WORDS FOR ABSTRACT: 222

CONFLICT OF INTEREST STATEMENT: The authors declare no competing financial interests.

ACKNOWLEDGEMENTS: Imperial College Skempton Scholarship to A.C. and Imperial College Research Fellowship to L.M.

Abstract

Our understanding of the behaviour of spinal alpha-motoneurons (MNs) in mammals partly relies on our knowledge of the relationships between MN membrane properties, such as MN size, resistance, rheobase, capacitance, time constant, axonal conduction velocity and afterhyperpolarization period. Qualitative relations between some of these properties are often assumed based on scattered but converging evidence from experimental studies and review papers.

We reprocessed the data from 40 experimental studies in adult cat, rat and mouse MN preparations *in vivo* to empirically derive precise mathematical relationships between MN electrophysiological and anatomical properties. This validated mathematical framework, which demonstrates that the MN membrane properties are all related to each other, expands our knowledge in neural electrophysiology beyond available literature data. For example, it extends the Henneman's size principle by the association between MN size and all other MN properties.

The derived mathematical relationships provide a convenient tool for neuroscientists and experimenters to estimate non-measurable MN properties, to explore relationships between pairs of MN properties never concurrently observed in previous experiments, to support future experimental investigations, or to investigate inter-mammalian-species variations in MN membrane properties. Using this mathematical framework, which supports the classic description of a MN as a membrane equivalent electrical circuit, modelers can build profiles of inter-consistent MN-specific properties to scale advanced models of MNs, with consequences on our understanding of the neural control of movement.

Keywords: motor neuron, motoneuron, motor neuron size, mathematical relationships, motor unit, Henneman's size principle

Introduction

Assessing the morphological and electrophysiological properties of individual spinal alpha-motoneurons (MNs) is crucial for understanding the recruitment and discharge behaviour of MNs and how the MN pool transforms the synaptic input into the muscle neural drive, and for exploring the neuro-mechanical interplay that controls voluntary motion in mammals. The studies that directly measured these properties in animals *in vivo* advanced our knowledge on spinal MNs by reporting significant correlations between some MN electrophysiological properties, such as the MN input resistance being strongly inversely associated to rheobase current (Krawitz et al., 2001; Button et al., 2008; Krutki et al., 2015; Huh et al., 2021).

Our knowledge on the associations between MN properties remains however limited as it currently relies on the qualitative interpretation of a series of datasets of small size that individually provide a crude and incomplete picture of MN physiological and biophysical features. It is indeed challenging to experimentally measure a complete and reliable set of MN-specific properties for a large sample of MNs because of technical difficulties in measuring MN morphometric and electrophysiological properties *in vivo*. Specialised experimental set-ups could measure a maximum of six MN properties concurrently in animal preparations, and for limited numbers of MNs (Gustafsson & Pinter, 1984a; Gustafsson & Pinter, 1984b).

For the above reasons, the statements reported in review papers on the associations between MN properties rely on converging conclusions from independent studies and remain speculative (Henneman, 1981; Burke, 1981; Binder et al., 1996; Powers & Binder, 2001; Kernell, 2006; Heckman & Enoka, 2012). While some qualitative associations, such as between MN size and resistance (Kernell & Zwaagstra, 1981; Burke et al., 1982), are commonly accepted and have led to extensions of the Henneman's size principle (Henneman, 1957; Wuerker et al., 1965; Henneman et al., 1965a; Henneman et al., 1965b; Henneman et al., 1974; Henneman, 1981; Henneman, 1985), these associations have never been quantitatively proven. Besides, other relationships, such as between MN size and membrane capacitance or time constant, are not known.

The limited knowledge on the associations between MN morphometric and/or electrophysiological quantities is detrimental for our understanding of individual MN behaviour and in computational models of a MN membrane equivalent electrical circuit (Izhikevich, 2004; Dong et al., 2011; Negro et al., 2016; Teeter et al., 2018). In these models, the MN property profiles, which are typically built with scattered data from a relatively small number of experimental studies, indicate reasonable orders of magnitude but are generic and result in a lack of inter-consistency between the MN properties. This approach yields obvious limitations when the sets of physiological and MN-specific characteristics

must be known for accurately interpreting the model predictions. Further investigating such associations between MN properties in mammals is therefore important to improve both our understanding of MN pool behaviour and the computational models of MNs.

Here, we derived and validated currently unknown mathematical relationships between all pairs of the MN morphometric and electrophysiological cat properties listed in Table 1 by reprocessing and merging the published data from 18 available experimental studies in adult cat preparations *in vivo*. In this way, we first demonstrate that the electrophysiological properties reported in Table 1 are all associated to each other and can be precisely predicted by MN size in cats. These mathematical relationships, which besides include quantified correlations between MN properties that were never concurrently measured in experiments, clarify our understanding of the neural electrophysiology beyond the experimental data available in the literature and can accelerate future research in the behaviour of individual MNs. They provide for the first time a mathematical framework, useful for neuroscientists, experimenters, and modelers, for the association between any pair of spinal MN properties and for the derivation of MN profiles of MN-specific morphometric and electrophysiological properties that reproduce published experimental mammal data *in vivo*.

Neuroscientists can use this mathematical framework to explore electrophysiological properties that cannot be measured, such as the MN specific input resistance and capacitance. Experimenters can directly compare their experimental measurements to other results published in the literature, which are described by the relationships, and can readily complete their datasets by deriving, with the provided relationships, consistent values for the MN properties that were not experimentally measured. Furthermore, these mathematical relationships can be a tool for modellers to advance the state-of-the-art in MN modelling by realistically scaling phenomenological models of individual MNs and building realistic and complete pools of individual MNs presenting continuously-varying electrophysiological profiles.

After deriving the mathematical framework from cat data, we then demonstrate that the normalized cat relationships apply to other mammals by validating them with data from 9 adult rat and mouse studies *in vivo*. This approach helps better understanding the inter-mammalian-species variations in MN properties and inferring MN profiles in humans, for example, in which most properties cannot be measured *in vivo*. Finally, using additional correlations obtained between some MN and muscle unit (mU) properties from 14 mammal studies, we discuss the empirical relationships obtained between MN properties in the context of the Henneman's size principle.

Table 1. The motoneuron (MN) and muscle unit (mU) properties investigated in this study with their notations and SI base units. S_{MN} is the size of the MN. As reproduced in Table 2, the MN size S_{MN} is adequately described by measures of the MN surface area S_{neuron} and the soma diameter D_{soma}. R and R_m define the MN-specific electrical resistance properties of the MN and set the value of the MN-specific current threshold I_{th} (Binder et al., 1996; Powers & Binder, 2001; Heckman & Enoka, 2012). C and C_m (constant among the MN pool) define the capacitance properties of the MN and contribute to the definition of the MN membrane time constant τ (Gustafsson & Pinter, 1984b; Zengel et al., 1985). ΔV_{th} is the constant amplitude of the membrane voltage depolarization threshold relative to resting state required to elicit an action potential. I_{th} is the corresponding electrical current causing a membrane depolarization of ΔV_{th}. AHP is defined in most studies as the duration between the action potential onset and the time at which the MN membrane potential meets the resting state after being hyperpolarized. ACV is the axonal conduction velocity of the elicited action potentials on the MN membrane. S_{mU} is the size of the mU. As indicated in Table 2, the mU size S_{mU} is adequately described by measures of (1) the sum of the cross-sectional areas (CSAs) of the fibres composing the mU CSA^{tot}, (2) the mean fibre CSA CSA^{mean}, (3) the innervation ratio IR, i.e. the number of innervated fibres constituting the mU, and (4) the mU tetanic force F^{tet}. The muscle force at which a mU starts producing mU force is called mU force recruitment threshold F^{th}.

	Properties	**Notation**	**Unit**
Motoneuron (MN) properties	Size:	S_{MN}	
	Neuron surface area	S_{neuron}	$[m^2]$
	Soma diameter	D_{soma}	$[m]$
	Resistance	R	$[\Omega]$
	Specific resistance per unit area	R_m	$[\Omega \cdot m^2]$
	Capacitance	C	$[F]$
	Specific capacitance per unit area	C_m	$[F \cdot m^{-2}]$
	Time constant	τ	$[s]$
	Rheobase (current recruitment threshold)	I_{th}	$[A]$
	Voltage threshold	ΔV_{th}	$[V]$
	Afterhyperpolarization period	AHP	$[s]$
	Conduction velocity	ACV	$[m \cdot s^{-1}]$
Muscle unit (mU) properties	Size:	S_{mU}	
	Total fibre cross-sectional area (CSA)	CSA^{tot}	$[m^2]$
	Mean fibre CSA	CSA^{mean}	$[m^2]$
	Innervation ratio	IR	[ ]
	Tetanic force	F^{tet}	$[N]$
	Force recruitment threshold	F^{th}	$[N]$

Methods

Studies reporting processable in vivo adult mammal data

To optimize inter-study analysis, we only selected studies that concurrently measured at least two of the morphometric and/or electrophysiological properties reported in Table 1 in individual spinal alpha-motoneurons of healthy adult cats, rats and mice observed *in vivo*. Larval and postnatal specimens were therefore disregarded because of the pronounced age-related variance (Highlander et al., 2020) in the mean values of the electrophysiological properties listed in Table 1, which corroborates the non-extrapolability of neonatal neuronal circuitry to older ages (Song et al., 2006; Carp et al., 2008; Nakanishi & Whelan, 2010; Mitra & Brownstone, 2012). Due to the nonlinear inter-species scalability of the spinal alpha-MN electrophysiological and morphometric properties (Manuel et al., 2019) and a pronounced variance in the inter-species mean values (Highlander et al., 2020), non-mammalian species were also disregarded, while the retained data from cats, rats and mice were processed separately. Highlander et al. (2020) also report an 'unexplained' variance in the mean property values reported between studies investigating specimens of the same species, sex and age, which may be explained by differences between *in vivo* and *in vitro* protocols (Carp et al., 2008). For this reason, only *in vivo* studies were considered, while most *in vitro* studies had already been disregarded at this stage as dominantly performed on neonatal specimens due to experimental constraints (Manuel et al., 2009a; Mitra & Brownstone, 2012).

To build an extensive set of relevant studies so that the mathematical relationships derived in this study describe a maximum of the data published in the literature, the output of the analysis provided in Highlander et al. (2020) was screened and used for a further search by reference lists. For convenience, in the following, the notation $\{A; B\}$ refers to the pair of morphometric or electrophysiological MN properties A and B, with $A, B \in \{S_{MN}; ACV; AHP; R; I_{th}; C;\ \tau\}$, defined in Table 1. The identified studies generally provided clouds of data points for pairs $\{A; B\}$ of concurrently measured MN properties through scatter graphs. These plots were digitized using the online tool WebPlotDigitizer (Ankit, 2020). When a study did not provide such processable data – most reported the mean $\pm SD$ property values of the cohort of measured MNs – the corresponding author was contacted to obtain the raw data of the measured MN properties, following approval of data sharing. Upon reception of data, datasets of all possible $\{A; B\}$ pairs were created and included into the study. As all but two selected studies focused on lumbosacral MNs, the final set of considered publications was constrained to MNs innervating hindlimb muscles to improve inter-study consistency.

From a preliminary screening of the retrieved studies, it was found that relatively more cat studies were obtained than rat and mouse studies, while the cat studies also investigated more $\{A; B\}$ pairs of morphometric and electrophysiological properties. The mathematical relationships sought in this paper between MN properties were thus derived from cat data, and the validated for extrapolation to rat and mouse data.

Relationships between MN properties

Normalized space

The sets of data retrieved from different cat studies for each property pair $\{A; B\}$ were merged into a 'global' dataset dedicated to that property pair. The $\{A; B\}$ data was also normalized for each study and transformed as a percentage of the maximum property value measured in the same study and normalized 'global' datasets were similarly created. A least squares linear regression analysis was performed for the $\ln(A) - \ln(B)$ transformation of each global dataset yielding relationships of the type $\ln(A) = a \cdot \ln(B) + k$, which were then converted into power relationships of the type $A = k \cdot B^a$ (eq.1). Power fitting was chosen for flexibility and simplicity. The adequacy of these global power trendlines and the statistical significance of the correlations were assessed with the coefficient of determination r^2 (squared value of the Pearson's correlation coefficient) and a threshold of 0.01 on the p-value of the regression analysis, respectively. For each $\{A; B\}$ pair, the normalized global datasets systematically returned both a higher r^2 and a lower p-value than the datasets of absolute $\{A; B\}$ values, in agreement with the 'unexplained' inter-experimental variance reported in (Highlander et al., 2020). It was therefore decided to investigate the $\{A; B\}$ pairs of MN properties in the normalized space using the normalized global datasets to improve the cross-study analysis.

Size-dependent normalized relationships

From inspection of the considered cat studies, most of the investigated MN property pairs comprised either a direct measurement of MN size, noted as S_{MN} in this study, or another variable strongly associated to size, such as axonal conduction velocity (ACV) or afterhyperpolarization period (AHP). Accordingly, and consistently with Henneman's size principle, we identified S_{MN} as the reference MN property with respect to which relationships with the electrophysiological MN properties in Table 1 were investigated.

To integrate the data from all global normalized datasets into the final relationships, the MN properties in Table 1 were processed in a step-by-step manner in the order $ACV, AHP, R, I_{th}, C, \tau$, as reproduced in Figure 1 for two arbitrary properties, to seek a 'final' power relationship of the type eq.1 between each of them and S_{MN}. For each electrophysiological property A and each $\{A; B\}$ dataset, we

considered two cases. If $B = S_{MN}$, the global dataset was not further processed as the electrophysiological property A was already related to MN size S_{MN} from experimental measurements. If $B \neq S_{MN}$, the global $\{A; B\}$ dataset was transformed into a new $\{A; S_{MN}\}$ dataset by converting the discrete values of B with the trendline regression $S_{MN} = k_d \cdot B^d$, which was obtained at a previous step of the data processing. With this dual approach, as many MN size-dependent $\{A; S_{MN}\}$ intermediary datasets as available $\{A; B\}$ global datasets were obtained for each property A. These size-dependent datasets were merged into a 'final' $\{A; S_{MN}\}$ dataset to which a least squares linear regression analysis was performed for the $\ln(A) - \ln(S_{MN})$ transformation, yielding relationships of the type $\ln(A) = c \cdot \ln(S_{MN}) + k$, which were converted into the power relationships:

$$A = k_c \cdot S_{MN}^c$$

The adequacy of these final power trendlines and the statistical significance of the correlations were assessed identically to the $\{A; B\}$ relationships derived directly from normalized experimental data, using the coefficient of determination r^2 (squared value of the Pearson's correlation coefficient) and a threshold of 0.01 on the p-value of the regression analysis, respectively. If $r^2 > 0.3$ (i.e. $r > 0.55$) and $p < 0.01$, another power trendline $S_{MN} = k_d \cdot A^d$ was fitted to the final dataset to describe the inverse relationship for $\{S_{MN}; A\}$ and used in the processing of the next-in-line property.

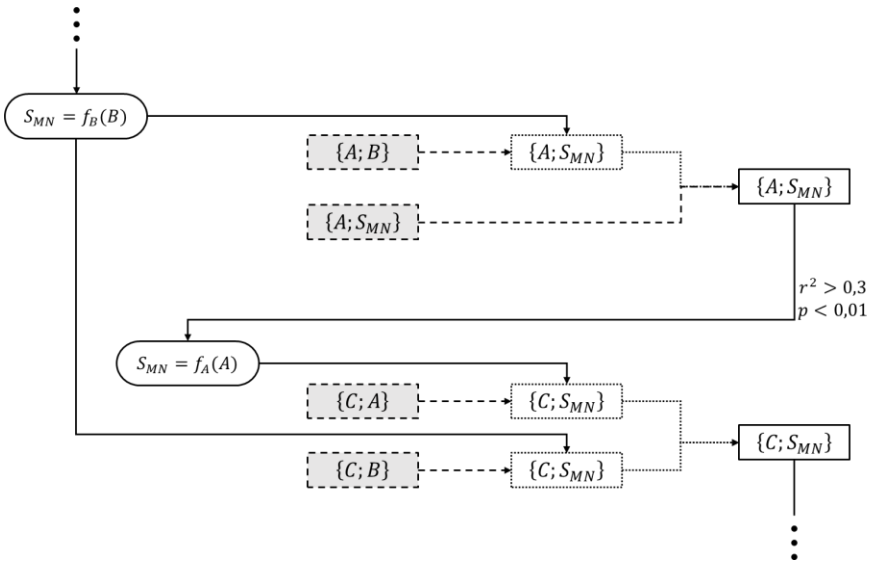

Figure 1. Two steps of the step-by-step approach to create the final MN size-related datasets. Here, the final $\{A; S_{MN}\}$ and $\{C; S_{MN}\}$ MN size-related datasets are created (right-side solid contour boxes), to which the final relationships $A, C = k_c \cdot S_{MN}^c$ were fitted. If $r^2 > 0.3$ and $p < 0.01$, power relationships $S_{MN} = f_A(A)$ and $S_{MN} = f_C(C)$ (oval boxes) were also fitted to the final $\{A; S_{MN}\}$ and $\{C; S_{MN}\}$ datasets. Here, $S_{MN} = f_B(B)$ was obtained from a previous unshown step. The normalized global datasets of experimental data (dashed-contour grey-filled boxes) were either directly included into the final datasets if already obtained as MN size-related, or first transformed into an MN size-related intermediary datasets (dotted-contour boxes) by converting the A and/or B properties into S_{MN} values with the $S_{MN} = f_A(A)$ and $S_{MN} = f_B(B)$ relationships. The final $\{A; S_{MN}\}$ and $\{C; S_{MN}\}$ MN size-related datasets were retained for further processing in this study.

Normalized mathematical relationships between electrophysiological properties

When a final relationship with S_{MN} was obtained for two MN properties A and B by the procedure described above, i.e., $A = k_{cA} \cdot S_{MN}^{c_A}$ and $B = k_{cB} \cdot S_{MN}^{c_B}$, one of the expressions was mathematically inverted and a third empirical relationship was derived for the property pair $\{A; B\}$:

$$A = \frac{k_{cA}}{(k_{cB})^{\frac{c_A}{c_B}}} \cdot (B)^{\frac{c_A}{c_B}} = k_e \cdot B^e$$

This procedure was applied to all possible $\{A; B\}$ pairs in Table 1.

Validation of the normalized relationships

The data in each $\{A; B\}$ global normalized dataset was initially randomized and therefore made independent from the studies constituting it. Each global dataset was then randomly split so that 70% of the data was processed to build the relationships, while the remaining 30% was used as a test dataset. The final size-related relationships $A = k_c \cdot S_{MN}^c$ and relationships between electrophysiological properties $A = k_e \cdot B^e$ were obtained as described previously using the 70%-datasets. These mathematical relationships were applied to the S_{MN} or B data in each 30%-dataset, yielding predicted values A. It was then assessed to what extent the mathematical relationships predicted the test data A by calculating the normalized maximum error (nME), the normalized root mean squared error ($nRMSE$) and the coefficient of determination r_{pred}^2 between predicted and control values of A in each 30%-dataset. This process was repeated for a total of 5 times, randomly creating novel 70-30 partitions of the global datasets. The nME, $nRMSE$ and r_{pred}^2 values were finally averaged across the five repetitions and the average r_{pred}^2 hence obtained was compared to the average of the r_{exp}^2 values obtained from the power trendlines least-squared fitted to the control data. This approach validated the relationships. Once validated with this cross-validation method, the final normalized size-dependent relationships $A = k_c \cdot S_{MN}^c$ and relationships between electrophysiological properties $A = k_e \cdot B^e$ were provided for the complete global datasets.

Scaling of the normalized relationships

The $A = k_c \cdot S_{MN}^c$ and $A = k_e \cdot B^e$ normalized relationships were finally scaled to typical cat property values in three steps. First, it was assessed from the literature the fold-range over which each MN property was to vary. S_{MN} varied over a q_S^E-fold range, taken as the average across cat studies of the ratios of minimum and maximum values measured for S_{MN}:

$$q_S^E = \frac{1}{N_{studies}} \sum_{i=1}^{N_{studies}} \left[\frac{(S_{MN_i})_{max}}{(S_{MN_i})_{min}} \right]$$

An experimental ratio q_A^E was similarly obtained for each electrophysiological property A. As $A = k_c \cdot S_{MN}^c$, any electrophysiological property A could theoretically vary over a $q_A^T = (q_S^E)^{|c|}$-fold range, which was compared to q_A^E for consistency in the results. Then, a theoretical range $[A_{min};\ A_{max}]$ of values were derived for each electrophysiological property A. Defining A_{min}^E and A_{max}^E as the respective average of the minimum and maximum A-values across studies, it was enforced $\frac{A_{max}}{A_{min}} = q_A^T$ and $\frac{A_{min}+A_{max}}{2} = \frac{A_{min}^E+A_{max}^E}{2}$ so that the $[A_{min};\ A_{max}]$ theoretical ranges were consistent with the normalized size-dependent relationships while best reproducing the experimental data from cat literature. A theoretical range for S_{MN} $[(S_{MN})_{min};\ (S_{MN})_{max}]$ was similarly built over the q_S^E-fold range previously derived. Finally, the intercept k_c in the size-dependent relationships $A = k_c \cdot S_{MN}^c$ was scaled as:

$$\begin{cases} k_c = \dfrac{A_{min}}{(S_{MN})_{min}^c} \ ; \ c > 0 \\ k_c = \dfrac{A_{max}}{(S_{MN})_{min}^c} \ ; \ c < 0 \end{cases}$$

A similar approach was used to mathematically derive the intercept k_e and scale the relationships $A = k_e \cdot B^e$ between electrophysiological properties.

<u>Extrapolation to rats and mice</u>

It was finally assessed whether the $A = k_c \cdot S_{MN}^c$ and $A = k_e \cdot B^e$ scaled relationships derived from cat data accurately predicted rat and mouse quantities reported in other experimental studies. These mathematical relationships were applied to the S_{MN} or B data in each $\{A; B\}$ global dataset of absolute values obtained for rats and mice independently. The accuracy in predicting the quantity A was assessed for each available dataset with the same three validation metrics used to validate the normalized power trend lines: the normalized maximum error (nME), the normalized root-mean-square error ($nRMSE$) and the coefficient of determination r^2 between predicted and experimental values of A.

Definitions of MN Size S_{MN} and mU size S_{mU}

<u>MN Size S_{MN}</u>

The identified papers that performed both electrophysiological and morphometric measurements on the same MNs dominantly measured the MN soma diameter D_{soma} as an index of MN size. Therefore, we choose $S_{MN} = D_{soma}$ in the described methodology. In the literature on spinal MNs in adult mammals *in vivo*, the size of a MN S_{MN} is also related to the measures of the somal cross-sectional area CSA_{soma} (Gao et al., 2009; Friese et al., 2009; Deardorff et al., 2013; Mierzejewska-Krzyżowska

et al., 2014; Dukkipati et al., 2018), soma surface area S_{soma} (Ulfhake, B. & Kellerth, 1984; Brandenburg et al., 2020), axonal diameter D_{axon} (Cullheim, 1978), individual dendrite diameter $D_{dendrite}$ (Amendola & Durand, 2008; Carrascal et al., 2009; Mantilla et al., 2018), individual dendritic surface area $S_{dendrite}$ (Li et al., 2005; Obregón et al., 2009; Carrascal et al., 2009; Filipchuk & Durand, 2012; Kanjhan et al., 2015), total dendritic surface area (Ulfhake, Brun & Cullheim, 1988; Amendola & Durand, 2008; Brandenburg et al., 2020) or total MN surface area S_{neuron} (Burke et al., 1982) defined as the summed soma and dendritic surface areas.

In the references (Zwaagstra & Kernell, 1981; Ulfhake & Kellerth, 1981), a linear correlation between D_{soma} and the average diameter of the stem dendrites $D_{dendrite_{mean}}$ has been reported ($r > 0.62$, population size in $\{40; 82\}$ cells). Moreover, a linear or quasi-linear correlation has been found (Cullheim et al., 1987; Ulfhake, Brun & Cullheim, 1988; Moschovakis et al., 1991; Prakash et al., 2000; Li et al., 2005; Obregón et al., 2009; Mantilla et al., 2018) between the stem dendrite diameter $D_{dendrite}$ and the membrane surface area of the corresponding dendritic tree $S_{dendrite}$ ($r > 0.78$, population size in $[33; 342]$ dendrites). Therefore, from these studies, we can assume an approximate linear correlation between D_{soma} and the average dendritic surface area $S_{dendrite_{mean}}$. Moreover, the number of dendritic trees $N_{dendrites}$ per cell increases with increasing soma surface S_{soma} (Brandenburg et al., 2018), and a linear correlation between D_{soma} or $S_{dendrites}$ with $N_{dendrites}$ has been observed (Zwaagstra & Kernell, 1981; Ulfhake, Brun & Cullheim, 1988; Amendola & Durand, 2008) ($r > 0.40$, population size in $\{14; 32; 87\}$ cells). It was therefore assumed that D_{soma} and total dendritic surface area $S_{dendrite}^{tot}$ are linearly correlated. This assumption/approximation is consistent other conclusions of a linear correlations between D_{soma} and $S_{dendrite}^{tot}$ (Amendola & Durand, 2008; Brandenburg et al., 2020). Then, according to typical values of D_{soma}, S_{soma} and $S_{dendrites}^{tot}$ obtained from the studies previously cited, yielding $S_{dendrites}^{tot} \gg S_{soma}$, it was also assumed $S_{dendrites}^{tot} \approx S_{neuron}$. It is thus concluded that D_{soma} is linearly related to total neuron membrane area S_{neuron}, consistently with results by Burke et al. (1982) ($r = 0.61$, 57 cells).

For the above reasons and assumptions, the mathematical relationships $A = k_c \cdot S_{MN}^c$ derived previously, with $S_{MN} = D_{soma}$, were extrapolated with a gain to relationships between A and $S_{MN} = S_{neuron}$, notably permitting the definition of surface specific resistance R_m and capacitance C_m. Following the same method as described above, theoretical ranges $[(S_{neuron})_{min}; (S_{neuron})_{max}]$ were derived from additional morphometric studies on adult cat spinal alpha-motoneurons. The new relationships were extrapolated as $A = k_c \cdot D_{soma}^c = \frac{(S_{neuron})_{min}}{(D_{neuron})_{min}} \cdot S_{neuron}^c$.

It must however be highlighted that the conclusion of a linear correlation between D_{soma} and S_{neuron}, while plausible, is crude. Morphometric measurements of individual MNs are indeed difficult and

285 suffer many limitations. MN staining, slice preparations and MN reconstruction and identification are
286 complex experimental procedures requiring a large amount of work; the results from most of the cited
287 studies thus rely on relatively small pools of investigated MNs. Most cited studies did not account for
288 tissue shrinkage after dehydration, while some may have failed to assess the full dendritic trees from
289 MN staining techniques (Brandenburg et al., 2020), thus underestimating dendritic membrane
290 measurements. Moreover, before automated tools for image segmentation, landmark mapping and
291 surface tracking (Amendola & Durand, 2008; Obregón et al., 2009; Mierzejewska-Krzyżowska et al.,
292 2014) were available, morphometric measurements were performed from the manual reproduction
293 of the cell outline under microscope, yielding important operator errors reported to be of the order of
294 $\sim 0.5 \mu m$, i.e. $\sim 20\%$ stem diameter. In these studies, morphologic quantities were besides obtained
295 from geometrical approximations of the 2D MN shape, such as modelling the individual dendritic
296 branches as one (Cullheim et al., 1987) or more (Prakash et al., 2000) equivalent cylinders for the
297 derivation of $S_{dendrite}$. Morphometric measurement approaches also varied between studies; for
298 example, oval or circle shapes were best fitted by sight onto the soma outline and equivalent D_{soma}
299 quantities were derived either as the mean of measured maximum and minimum oval diameters or as
300 the equivalent diameter of the fitted circle. In these studies, CSA_{soma} and S_{soma} were therefore
301 derived by classical equations of circle and spheric surface areas, which contradicts the results by
302 Mierzejewska-Krzyżowska et al. (2014) obtained from surface segmentation of a linear relationship
303 between D_{soma} and CSA_{soma} ($r = 0.94$, 527 MNs). Finally, no correlation between soma size and
304 $N_{dendrites}$ was found (Ulfhake & Kellerth, 1981; Cullheim et al., 1987). Therefore, the linear correlation
305 between D_{soma} and S_{neuron} is plausible but crude and requires awareness of several important
306 experimental limitations and inaccuracies. Conclusions and predictions involving S_{neuron} should be
307 treated with care in this study as these morphometric measurements lack the precision of the
308 measures performed for the electrophysiological properties listed in Table 1.

309 Muscle unit size S_{mU}

310 To enable future comparisons between MN and mU properties, we here assess potential indices of the
311 mU size S_{mU} suggested in the literature. The size of a mU (S_{mU}) can be defined as the sum CSA^{tot} of
312 the cross-sectional areas CSAs of the innervated fibres composing the mU. CSA^{tot} depends on the mU
313 innervation ratio (IR) and on the mean CSA (CSA^{mean}) of the innervated fibres: $S_{mU} = CSA^{tot} = IR \cdot$
314 CSA^{mean}. CSA^{tot} was measured in a few studies on cat and rat muscles, either indirectly by
315 histochemical fibre profiling (Burke & Tsairis, 1973; Dum & Kennedy, 1980; Burke, 1981), or directly by
316 glycogen depletion, periodic acid Schiff (PAS) staining and fibre counting (Burke et al., 1982; Rafuse et
317 al., 1997). The mU tetanic force F^{tet} is however more commonly measured in animals. As the fibre
318 mean specific force σ is considered constant among the mUs of one muscle in animals (Lucas et al.,

1987; Enoka, 1995), the popular equation $F^{tet} = \sigma \cdot IR \cdot CSA^{mean}$ (Burke, 1981; Enoka, 1995) returns a linear correlation between F^{tet} and $IR \cdot CSA^{mean} = S_{mU}$ in mammals. Experimental results (Burke & Tsairis, 1973; Bodine et al., 1987; Chamberlain & Lewis, 1989; Kanda & Hashizume, 1992; Rafuse et al., 1997; Hegedus et al., 2007) further show a linear correlation between F^{tet} and IR and between F^{tet} and CSA^{mean}. Consequently, F^{tet}, IR and CSA^{mean} are measurable, consistent, and linearly related measures of S_{mU} in animals, as summarized in Table 2.

Table 2. Measurable indices of MN and mU sizes in mammals. S_{MN} and S_{mU} are conceptual parameters which are adequately described by the measurable and linearly inter-related quantities reported in this table.

MN size ($\boldsymbol{S_{MN}}$)	mU size ($\boldsymbol{S_{mU}}$)
$\boldsymbol{S_{neuron}}$	F^{tet}
$\boldsymbol{D_{soma}}$	IR
	CSA^{mean}
	CSA^{tot}

Relationships between MN and mU properties

To assess whether the size-dependent relationships $A = k_c \cdot S_{MN}^c$ derived in this study were in accordance with Henneman's size principle of motor unit recruitment, we identified a set of experimental studies that concurrently measured a MN property B_{MN} (Table 1) and a muscle unit (mU) property A_{mU} for the same MU. The normalized global datasets obtained for the pairs $\{A_{mU}; B_{MN}\}$ were fitted with power trendlines, as previously described for MN properties, yielding $A_{mU} = k \cdot B_{MN}^b$ relationships. Using both the definition of S_{mU} (Table 2) and the $A = k_c \cdot S_{MN}^c$ relationships derived previously, the $A_{mU} = k \cdot B_{MN}^b$ relationships were then mathematically transformed into $S_{mU} = k \cdot S_{MN}^c$ relationships. If all c-values obtained from different $\{A_{mU}; B_{MN}\}$ pairs were of the same sign, it was concluded that mU and MN sizes were monotonically related. Considering the limited data available obtained from the literature, data obtained for MNs innervating different hindlimb muscles were merged. Also, cat, rat and mouse studies were processed independently but the resulting c-values were compared without regards to the related species.

Results

We respectively identified 18, 6 and 4 studies respecting our desired criteria on cats, rats and mice that reported processable experimental data for the morphometric and electrophysiological properties listed in Table 1. Additional publications including some from the past 10 years were identified but could not be included in this work as no processable data could be recovered. An additional 14 studies were found to perform concurrent MN and mU measurements on individual motor units.

From the selected cat studies, the 17 pairs of MN properties and the 8 pairs of one MN and one mU property represented in the bubble diagram of Figure 2A were investigated.

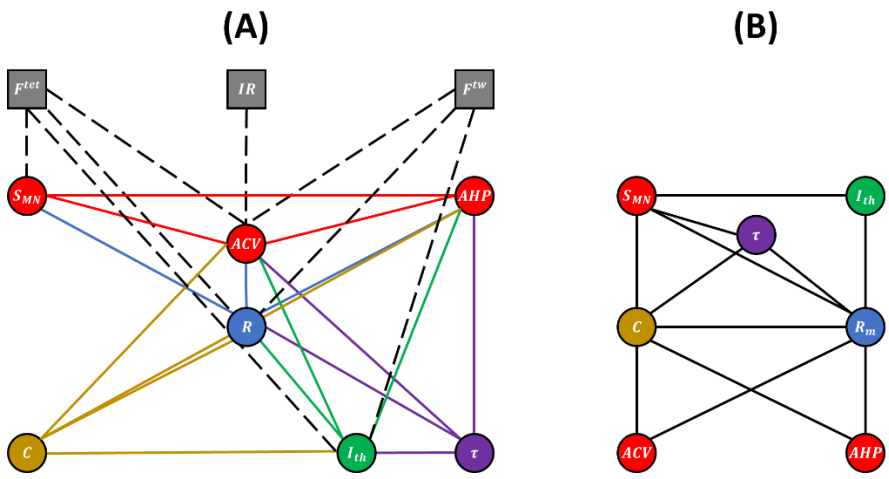

Figure 2. Experimental (A) and unknown (B) relations between MN and mU properties. (A) Bubble diagram representing the pairs of MN and/or mU properties that could be investigated in this study from the results provided by the 40 studies identified in our web search. MN and mU properties are represented in circle and square bubbles, respectively. Relationships between MN properties are represented by coloured connecting lines; the colours red, blue, green, yellow, and purple are consistent with the order $ACV, AHP, R, I_{th}, C, \tau$ in which the pairs were investigated (see Table 3 for mathematical relationships). Relationships between one MN and one mU property are represented by black dashed lines. (B) Bubble diagram representing the mathematical relationships proposed in this study between pairs of MN properties for which no concurrent experimental data has been measured to date.

Relationships between MN properties

<u>Studies providing cat data</u>

All 18 studies focusing on cats included in this work were published between 1966 and 2001. They applied similar experimental protocols. Briefly, animals were anesthetized, immobilized, and kept under artificial breathing. Hindlimb muscles of interest were dissected free, and their nerves were mounted onto stimulating electrodes, while maintaining body temperature between 35°C and 38°C.

After a laminectomy was performed over the lumbosacral region of the spinal cord, the MNs were identified by antidromic invasion following electrical stimulation of the corresponding muscle nerves. All studies reported the use of electrodes having stable resistances and being able to pass currents up to 10 nA without evident polarization or rectification. Most studies performed intracellular recordings using similar experimental approaches for the measurements of the electrophysiological parameters. For instance, all studies measured the MN membrane input resistance using the spike height method (Frank & Fuortes, 1956) by measuring the effects of steady currents, injected through the intracellular microelectrode, on the amplitude of antidromic spikes. Some aspects of the experimental protocol however diverged between studies, such as the age and the sex of the group of adult cats, the size population of cats and recorded MNs, the muscles innervated by the recorded MNs, the means of anaesthesia, the level of oxygen, and whether the spinal dorsal roots were severed (Kernell, 1966; Burke, 1968; Barrett & Crill, 1974; Fleshman et al., 1981; Gustafsson & Pinter, 1984a; Gustafsson & Pinter, 1984b; Zengel et al., 1985; Foehring et al., 1987), the complete surrounding hindlimbs were denervated (Burke, 1968; Kernell & Zwaagstra, 1981) or the spinal cord was transected (Burke, 1968; Krawitz et al., 2001). All the selected studies performing morphometric measurements injected the recorded MNs intracellularly with horseradish peroxidase (HRP) tracer by applying a continuous train of anodal current pulses. The spinal cord was eventually sliced frozen or at room temperature with a microtome or a vibratome and the MN morphometry was investigated. All morphometric measurements were manually performed, and the MN compartments (soma, dendrites, axon) approached by simple geometrical shapes, yielding the limitations previously listed.

Normalized relationships

The experimental data retrieved for the 17 pairs of MN properties drawn in Figure 2A were successfully digitized and merged into 17 normalized global datasets as reproduced in Figure 3. For information, power trendlines were fitted to these normalized datasets and reported in Table 3. All 17 trendlines were statistically significant, showing inter-study consistency in normalized measurements, and adequately represented by a power model $A = k_a \cdot B^a$ (p-value$< 10^{-5}$ and $r^2 \in [0.34; 0.72]$ for 15 datasets; p-value$< 10^{-5}$ and $r^2 \in \{0.24; 0.17\}$ for the $\{C; AHP\}$ and $\{C; CV\}$ datasets respectively).

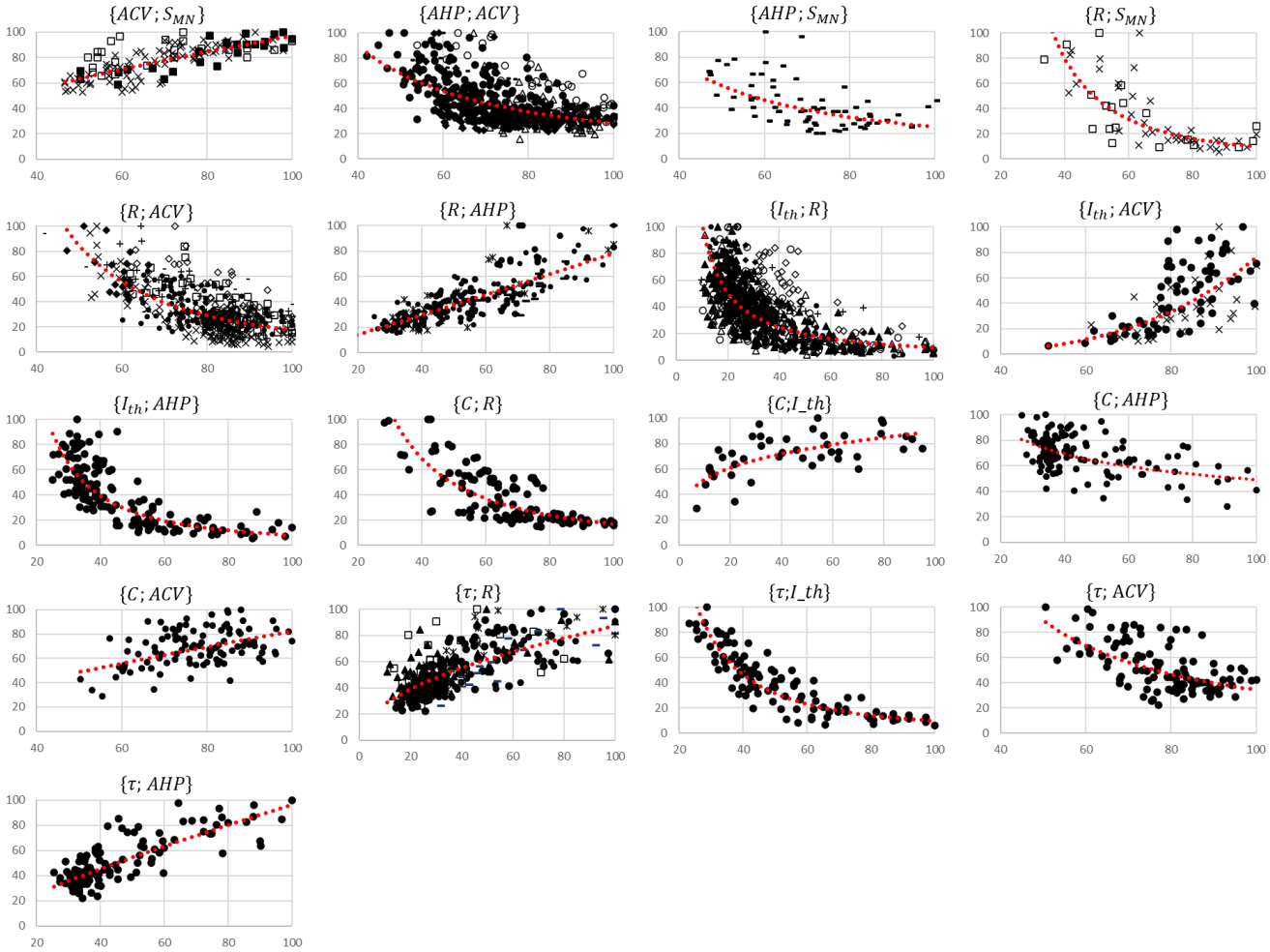

Figure 3. Normalized global datasets. These are obtained from the 18 studies reporting cat data that measured and investigated the 17 pairs of MN properties reported in Figure 2A. For each $\{A; B\}$ pair, the property A is read on the y axis and B on the x axis. For information, power trendlines $A = k \cdot B^a$ (red dotted curves) are fitted to the data of each dataset and reported in Table 3. The studies are identified with the following symbols: • (Gustafsson, B., 1979; Gustafsson & Pinter, 1984a; Gustafsson & Pinter, 1984b), ○ (Munson et al., 1986), ▲ (Zengel et al., 1985), Δ (Foehring et al., 1987), ■ (Cullheim, 1978), □ (Burke, 1968; Burke & Ten Bruggencate, 1971; Burke et al., 1982), ◆ (Krawitz et al., 2001), ◇ (Fleshman et al., 1981), + (Kernell, 1966), ╳ (Kernell & Zwaagstra, 1981; Kernell & Monster, 1981), - (Zwaagstra, B. & Kernell, 1980), — (Sasaki, 1991), ✶ (Pinter & Vanden Noven, 1989). The axes are given in % of the maximum retrieved values in the studies consistently with the Methods section.

The 17 normalized global datasets were processed according to the Methods to derive normalized mathematical relationships between the electrophysiological properties listed in Table 1 and MN size S_{MN}. First, the normalized size-dependent relationship $ACV = 4.0 \cdot S_{MN}^{0.7}$, reported in Table 3, was derived from the trendline fitting of the normalized $\{ACV; S_{MN}\}$ dataset, which was obtained from 3 studies (Cullheim, 1978; Kernell & Zwaagstra, 1981; Burke et al., 1982) and is represented in the upper-left panel in Figure 3. This resulted in a statistically significant relationship ($r^2 = 0.58$, p-value$< 10^{-5}$). A statistically significant ($r^2 = 0.59$, p-value$< 10^{-5}$) inverse relationship $S_{MN} = k_d \cdot ACV^d$ was also fitted to this dataset. Then, the $\{AHP; ACV\}$ dataset, represented in the second panel upper row in Figure 3 and obtained from 3 studies (Zwaagstra, B. & Kernell, 1980; Gustafsson & Pinter, 1984a; Foehring et al., 1987) was transformed into a new $\{AHP; S_{MN}\}_1$ dataset by applying the priory derived $S_{MN} = k_d \cdot ACV^d$ relationship to the list of ACV-values. This transformed $\{AHP; S_{MN}\}_1$ dataset was then merged with the $\{AHP; S_{MN}\}_2$ dataset (third panel upper row in Figure 2) obtained from (Zwaagstra, B. & Kernell, 1980), yielding the final $\{AHP; S_{MN}\}_f$ dataset of $N = 492$ data points shown in Figure 4, second panel. A statistically significant ($r^2 = 0.58$, p-value$< 10^{-5}$) power trendline $AHP = 2.5 \cdot 10^4 \cdot S_{MN}^{-1.5}$ was fitted to the $\{AHP; S_{MN}\}_f$ dataset and is reported in Table 3. As before, a statistically significant ($r^2 = 0.38$, p-value$< 10^{-5}$) inverse relationship $S_{MN} = k_d \cdot AHP^d$ was also fitted to this dataset for future use. A similar procedure was applied to derive the normalized final relationships between $\{R, I_{th}, C, \tau\}$ and S_{MN} reported in the last column of Table 3. A statistically significant (p-value$< 10^{-5}$) correlation was obtained between each electrophysiological property $\{ACV, AHP, R, I_{th}, C, \tau\}$ and S_{MN} as reported in Table 3. With $r^2 \in [0.28; 0.58]$, it was obtained that $\{I_{th}, C, CV\}$ and $\{R, AHP, \tau\}$ respectively increased and decreased with increasing MN sizes S_{MN}, with slopes reported in Table 3 and visually displayed in Figure 5.

Table 3. Fitted experimental data of pairs of MN properties and subsequent normalized final size-related relationships. For information, the r^2, p-value and the equation $A = k_a \cdot B^a$ are reported for each fitted global dataset. The normalized MN-size dependent relationships $A = k_c \cdot S_{MN}^c$ are mathematically derived from the transformation of the global datasets and from the power trendline fitting of the final datasets (N data points) as described in the Methods.

MN property	$A = k_a \cdot B^a$ (normalized global datasets)						$A = k_c \cdot S_{MN}^c$ (final MN-size dependent datasets)				
A	Relationship	k_a	a	r^2	p-value	Reference studies	k_c	c	r^2	p-value	N points
ACV	$ACV = k_a \cdot S_{MN}^a$	4.0	0.7	0.58	$p < 10^{-5}$	(Cullheim, 1978; Kernell & Zwaagstra, 1981; Burke et al., 1982)	4.0	0.7	0.58	$p < 10^{-5}$	109
AHP	$AHP = k_a \cdot S_{MN}^a$	$6.1 \cdot 10^3$	-1.2	0.34	$p < 10^{-5}$	(Zwaagstra, B. & Kernell, 1980)	$2.5 \cdot 10^4$	-1.5	0.41	$p < 10^{-5}$	492
	$AHP = k_a \cdot ACV^a$	$1.5 \cdot 10^4$	-1.4	0.43	$p < 10^{-5}$	(Zwaagstra, B. & Kernell, 1980; Gustafsson & Pinter, 1984a; Foehring et al., 1987)					
R	$R = k_a \cdot S_{MN}^a$	$1.5 \cdot 10^5$	-2.1	0.61	$p < 10^{-5}$	(Kernell & Zwaagstra, 1981; Burke et al., 1982)	$9.6 \cdot 10^5$	-2.4	0.37	$p < 10^{-5}$	745
	$R = k_a \cdot ACV^a$	$6.3 \cdot 10^4$	-2.3	0.40	$p < 10^{-5}$	(Kernell, 1966; Burke, 1968; Barrett & Crill, 1974; Kernell & Zwaagstra, 1981; Fleshman et al., 1981; Gustafsson & Pinter, 1984a; Sasaki, 1991)					
	$R = k_a \cdot AHP^a$	$6.2 \cdot 10^{-1}$	1.1	0.65	$p < 10^{-5}$	(Gustafsson, B., 1979; Gustafsson & Pinter, 1984a; Foehring et al., 1987; Pinter & Vanden Noven, 1989; Sasaki, 1991)					
I_{th}	$I_{th} = k_a \cdot R^a$	$1.1 \cdot 10^3$	-1.0	0.37	$p < 10^{-5}$	(Kernell, 1966; Fleshman et al., 1981; Gustafsson & Pinter, 1984b; Zengel et al., 1985; Munson et al., 1986; Foehring et al., 1987; Krawitz et al., 2001)	$9.0 \cdot 10^{-4}$	2.5	0.37	$p < 10^{-5}$	722
	$I_{th} = k_a \cdot ACV^a$	$3.2 \cdot 10^{-6}$	3.7	0.37	$p < 10^{-5}$	(Kernell & Monster, 1981; Gustafsson & Pinter, 1984b)					
	$I_{th} = k_a \cdot AHP^a$	$2.5 \cdot 10^4$	-1.7	0.60	$p < 10^{-5}$	(Gustafsson & Pinter, 1984b)					
C	$C = k_a \cdot R^a$	$2.4 \cdot 10^2$	-0.4	0.57	$p < 10^{-5}$	(Gustafsson & Pinter, 1984a)	1.2	1.0	0.28	$p < 10^{-5}$	444
	$C = k_a \cdot I_{th}^a$	$2.9 \cdot 10^1$	0.26	0.51	$p < 10^{-5}$	(Gustafsson & Pinter, 1984b)					
	$C = k_a \cdot AHP^a$	$2.8 \cdot 10^2$	-0.4	0.24	$p < 10^{-5}$	(Gustafsson & Pinter, 1984a)					
	$C = k_a \cdot ACV^a$	2.5	0.8	0.17	$p < 10^{-5}$	(Gustafsson & Pinter, 1984a)					
τ	$\tau = k_a \cdot R^a$	8.7	0.5	0.52	$p < 10^{-5}$	(Burke & Ten Bruggencate, 1971; Barrett & Crill, 1974; Gustafsson, B., 1979; Gustafsson & Pinter, 1984a; Zengel et al., 1985; Pinter & Vanden Noven, 1989; Sasaki, 1991)	$2.6 \cdot 10^4$	-1.5	0.46	$p < 10^{-5}$	649
	$\tau = k_a \cdot AHP^a$	2.2	0.8	0.63	$p < 10^{-5}$	(Gustafsson & Pinter, 1984a)					
	$\tau = k_a \cdot I_{th}^a$	$2.3 \cdot 10^2$	-0.45	0.72	$p < 10^{-5}$	(Gustafsson & Pinter, 1984b)					
	$\tau = k_a \cdot ACV^a$	$1.2 \cdot 10^4$	-1.3	0.30	$p < 10^{-5}$	(Gustafsson & Pinter, 1984a)					

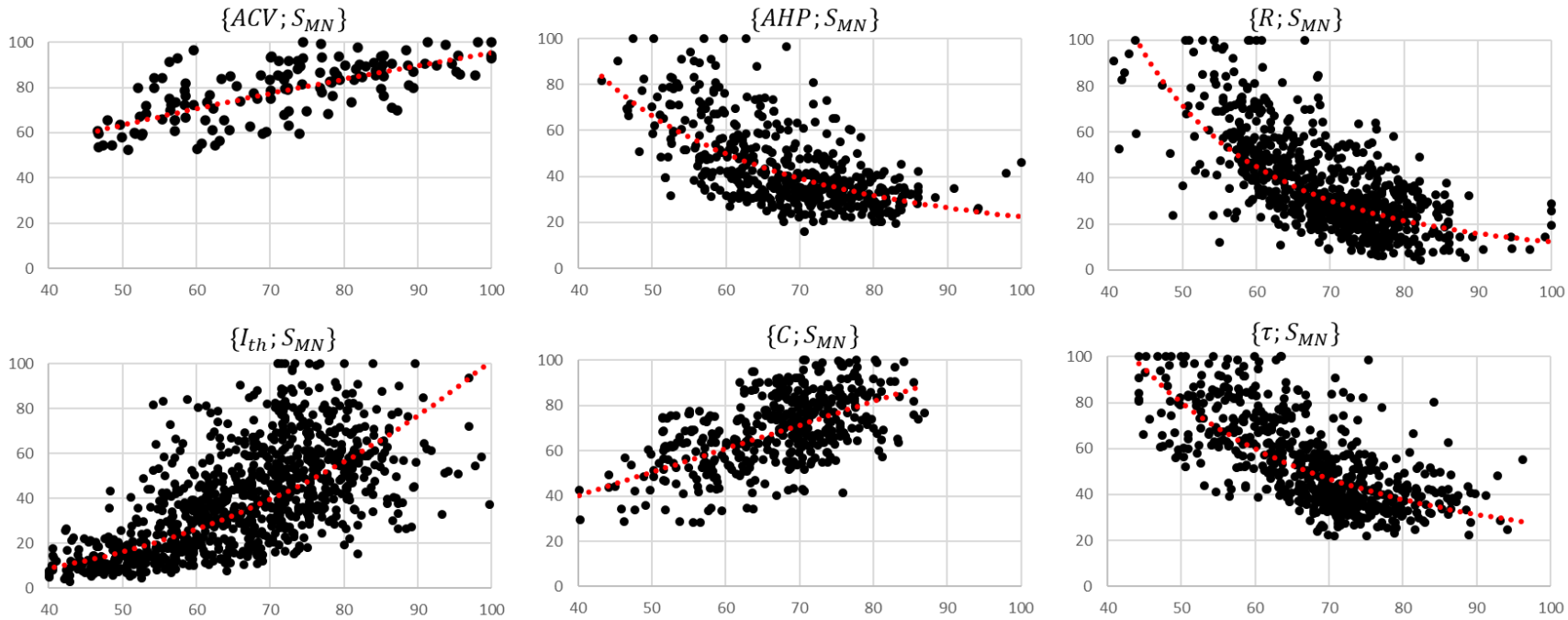

Figure 4. Normalized MN size-related final datasets. These are obtained from the 18 studies reporting cat data that concurrently measured at least two of the morphometric and electrophysiological properties listed in Table 1. For each $\{A; S_{MN}\}$ pair, the property A is read on the y axis and S_{MN} on the x axis. The power trendlines $A = k_c \cdot S_{MN}^c$ (red dotted curves) are fitted to each dataset and are reported in Table 3.

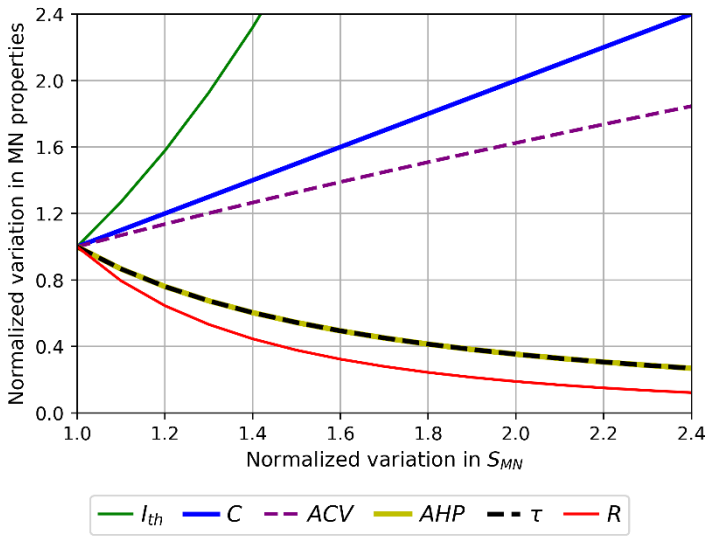

Figure 5. Normalized size-dependent behaviour of the MN properties ACV, AHP, R, I_{th}, C and τ. For displaying purposes, the MN properties are plotted in arbitrary units as power functions (intercept $k = 1$) of S_{MN}: $A = S_{MN}^{c}$ according to Table 3. The larger the MN size, the larger ACV, C and I_{th} in the order of increasing slopes, and the lower AHP, τ and R in the order of increasing slopes.

Normalized mathematical relationships between electrophysiological properties

The final size-dependent relationships reported in Table 3 were mathematically combined to yield normalized relationships between all electrophysiological properties listed in Table 1. As an example, $I_{th} = 9.4 \cdot 10^{-4} \cdot S_{MN}^{2.5}$ and $R = 9.6 \cdot 10^{5} \cdot S_{MN}^{-2.4}$ were obtained in Table 3. When mathematically combined (with the latter mathematically inverted as $S_{MN} = 2.9 \cdot 10^{2} \cdot R^{-0.4}$), these relationships yielded the normalized relationship between rheobase and input resistance $I_{th} = 1.5 \cdot 10^{3} \cdot R^{-1}$. All normalized relationships between MN electrophysiological properties hence obtained are provided in Supplementary Material.

Validation of the normalized relationships

The procedure and normalized relationships reported in Table 3 were obtained from the complete global datasets represented in Figure 3. To provide a validation of this approach and of the normalized relationships, the global datasets were split into two random partitions respectively containing 70% and 30% of the data, after the data points order was randomized within each dataset. Normalized relationships between $\{CV, AHP, R, I_{th}, C, \tau\}$ and S_{MN}, and then between all electrophysiological properties were derived from the 70%-datasets following the same procedure as previously described, and their predictions compared to the ground truth 30%-datasets with calculations of the $nME, nRMSE$ and r_{pred}^{2} validation metrics. This validation was performed for five random 70%-30% partitions of the global datasets. Figure 6 reports the average $nME, nRMSE$ and r_{pred}^{2} values across the five trials. The coefficient of determination between experimental and predicted quantities was

besides compared to the r^2_{exp}-value of the power trendline best fitted to the experimental data directly, which provides the highest r^2 value possibly reachable by our model. As displayed in Figure 6, the normalized relationships obtained from the 17 70%-datasets predicted the experimental data from the 30%-datasets with average nME between 48% and 412%, 12% to 26% $nRMSE$ and coefficients of determination r^2_{pred} that diverged from the higher limit r^2_{exp} by a maximum of 7% (for the $\{R; ACV\}$ pair in Figure 6). These results confirm the validity of the obtained relationships.

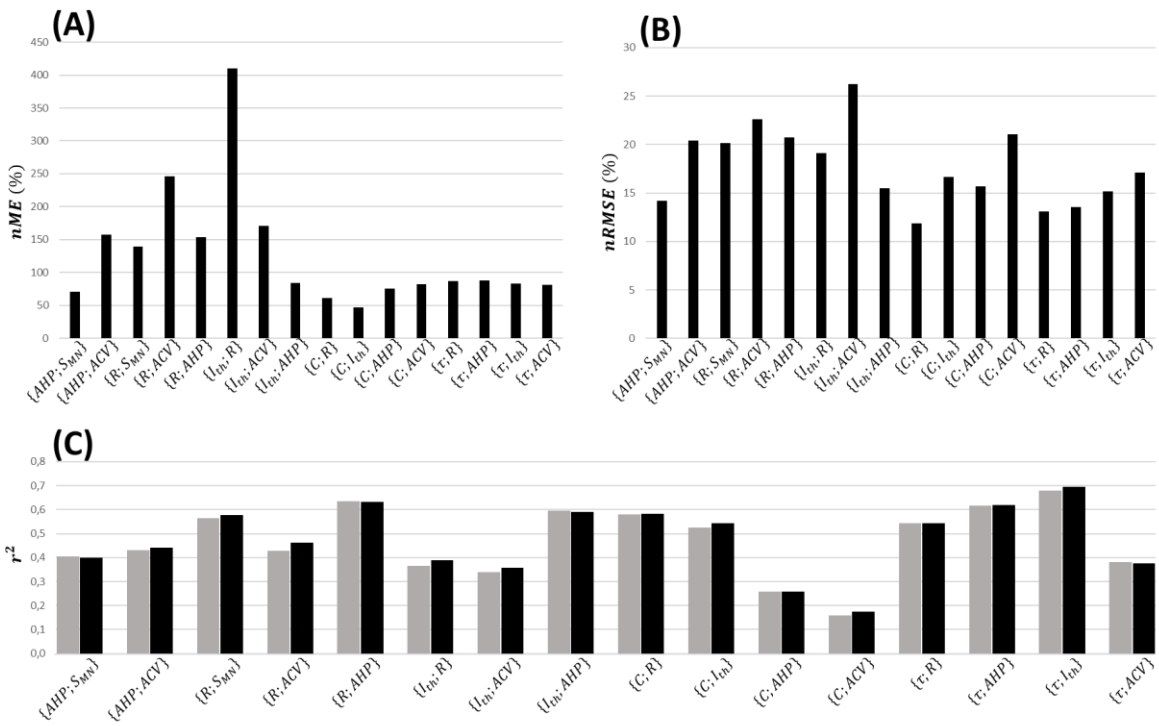

Figure 6. Validation of the normalized mathematical relationships obtained from the 70%-datasets against the corresponding 30%-datasets. For each 30%-dataset are reported the average values across the five trials of (A) the normalized maximum error (nME), (B) the normalized root-mean-square error ($nRMSE$), and (C) coefficient of determination (r^2_{pred}, grey bars) which is compared with the coefficient of determination (r^2_{exp}, black bars) of the power trendline fitted to the experimental data directly.

The normalized relationships reported in Supplementary material (and in Table 6 after scaling) were also strongly consistent with other experimental data in cats that were not included in the global datasets displayed in Figure 3 and used for deriving the normalized relationships. The normalized relationships $I^{th} = k \cdot \tau^{-1.7}$, $\frac{1}{C} = k \cdot \tau^{0.6}$, $\frac{1}{S_{MN}} = k \cdot CV^{-1.4}$ and $\frac{1}{R} = k \cdot CV^{3.5}$ yielded, when combined, $\frac{I^{th}}{C} = k \cdot \tau^{-1.1}$ and $\frac{1}{R \cdot S_{MN}} = k \cdot CV^{2.1}$, which are consistent with the relationship $\frac{I^{th}}{C} = k \cdot \tau^{-1}$ experimentally observed by Gustafsson & Pinter (1985) and $\frac{1}{R \cdot S_{MN}} = k \cdot CV^{1.9}$ measured by Kernell & Zwaagstra (1981). The stronger-than-linear inverse relationship $R = k \cdot S_{MN}^{-2.4}$ is also consistent with the phenomenological conclusions by Kernell & Zwaagstra (1981).

476 Scaling of the normalized relationships

477 The normalized relationships provided in Supplementary Material were finally scaled to typical cat data
478 obtained from the literature following the procedure described in the Methods section. D_{soma} and
479 S_{neuron} were found to vary in cats over an average $q_S^E = 2.4$-fold range according to a review of the
480 morphometric studies reported in the two first lines of Table 4. The similar ranges obtained for these
481 two morphometric quantities support the findings of the linear inter-relationship existing between
482 them and justified in the Methods.

483 It must however be noted that the minimum and maximum values of S_{neuron} and D_{soma} reported in
484 Table 4 may underestimate the true distribution of MN sizes in a MN pool for several reasons. First,
485 the studies reported in Table 4 investigated MN populations of small size, so that the largest and
486 smallest MNs of the investigated MN pools may not have been systematically identified and measured.
487 Also, dendritic labelling by staining may only identify dendrites up to the 3rd dendritic branch (Issa et
488 al., 2010; Fogarty et al., 2018) and full dendritic trees may not be identified, thus underestimating
489 S_{neuron} for the largest MNs that exhibit the highest dendritic tree complexity (Fogarty et al., 2020).
490 Finally, the distribution of gamma- and alpha-MN sizes is typically bimodal and the size distributions
491 of the two populations are reported to overlap (Moschovakis et al., 1991; von Steyern et al., 1999;
492 Friese et al., 2009; Deardorff et al., 2013). However, most studies reported in Table 4 identify the alpha
493 MNs from the gamma MNs by visually splitting the bimodal distributions of MN sizes in two
494 independent domains (Donselaar et al., 1986; Ishihara et al., 2001), thus neglecting the overlap.
495 Similarly, some studies identify as gamma MNs any MN showing an axonal conduction velocity typically
496 less than $\sim 60 m \cdot s^{-1}$ (Zwaagstra, B. & Kernell, 1980; Ulfhake, B. & Kellerth, 1984). These approaches
497 lead to overestimating the lower limit for the reported D_{soma} and S_{neuron} values. Consequently, true
498 ranges in MN sizes may be larger than the theoretical ones reported in Table 4. A similar comment can
499 be made for the electrophysiological properties reported in Table 5.

500 However, the $q_S^E = 2.4$-fold range obtained for cats is consistent with the fold-ranges obtained from
501 rat and mouse data for D_{soma} as reported in Table 4, while it underestimates the 4.4-fold range in
502 S_{neuron} values observed in mice. Table 4 finally shows that typical cat MN sizes are larger than in rats
503 and mice respectively, as reviewed by Manuel et al. (2019).

504

Table 4. Typical ranges of physiological values for $\boldsymbol{D_{soma}}$ and $\boldsymbol{S_{neuron}}$ in cat rat and mouse species. S_{MN} is found to vary over an average $q_S^E = 2.4$-fold range, which sets the amplitude of the theoretical ranges. Absolute {min; max} reports the minimum and maximum values retrieved in the reference studies for D_{soma} and S_{neuron}, while average {min; max} is obtained as the average across reference studies of minimum and maximum values retrieved per study.

	Property	Unit	Absolute {min;max}	Average {min; max}	q_S^E	Reference studies	Theoretical range
Cat	$\boldsymbol{D_{soma}}$	$[\mu m]$	$\{25.0; 90.0\}$	$\{36.7; 75.5\}$	2.2	(Kernell, 1966; Cullheim, 1978; Zwaagstra, B. & Kernell, 1980; Kernell & Zwaagstra, 1981; Ulfhake & Kellerth, 1981; Zwaagstra & Kernell, 1981; Burke et al., 1982; Donselaar et al., 1986; Destombes et al., 1992)	$[33; 79]$
	$\boldsymbol{S_{neuron}}$	$[mm^2]$	$\{0.08; 0.64\}$	$\{0.17; 0.45\}$	2.7	(Barrett & Crill, 1974; Ulfhake & Kellerth, 1981; Burke et al., 1982; Ulfhake, B. & Kellerth, 1984; Ulfhake, Brun & Cullheim, 1988; Moschovakis et al., 1991)	$[0.18; 0.44]$
Rat	$\boldsymbol{D_{soma}}$	$[\mu m]$	$\{17.5; 66.0\}$	$\{23.9; 55.7\}$	2.4	(Swett et al., 1986; von Steyern et al., 1999; Copray & Kernell, 2000; Ishihara et al., 2001; Deardorff et al., 2013; Mierzejewska-Krzyżowska et al., 2014)	
Mouse	$\boldsymbol{D_{soma}}$	$[\mu m]$	$\{14.0; 35.0\}$	$\{14.0; 35.0\}$	2.5	(von Steyern et al., 1999)	
	$\boldsymbol{S_{neuron}}$	$[mm^2]$	$\{0.01; 0.08\}$	$\{0.01; 0.06\}$	4.4	(Amendola & Durand, 2008; Brandenburg et al., 2020)	

Then, the empirical q_A^E and theoretical q_A^T ratios, defined in the Methods, were calculated for each MN electrophysiological property A and are reported in Table 5. For example, MN resistance R was found to vary over an average $q_R^E = 10.9$-fold range in a MN pool according to the literature, while the theoretical fold range $q_R^T = (q_S^E)^{|c_R|} = 2.4^{2.4} = 8.4$ was obtained from the $R = 9.6 \cdot 10^5 \cdot S_{MN}^{-2.4}$ normalized relationship previously derived when a 2.4-fold range is set for S_{MN}. As shown in Table 5, $\frac{q_A^E}{q_A^T} \in [0.8; 1.3]$ for the MN properties $C, \tau,\ AHP$ and ACV, while the theoretical ranges for R and I_{th} span over a narrower domain than expected from experimental results. The latter either suggests an underestimation of the MN q_S^E-fold range as discussed previously or of the power c in the relationships $I_{th}, R = k_c \cdot S_{MN}^c$.

Table 5: Typical ranges of physiological values for the MN properties $\boldsymbol{R}, \boldsymbol{R_m}, \boldsymbol{C}, \boldsymbol{\tau}, \boldsymbol{I_{th}}, \boldsymbol{AHP}$ and $\boldsymbol{ACV}$. As described in the Methods section, q_A^E is the average among reference studies of the ratios of minimum and maximum values; the properties experimentally vary over a q_A^E-fold range. This ratio compares with the theoretical ratio $q_A^T = (q_S^E)^{|c|}$ (with c taken from Table 3), which sets the amplitude of the theoretical ranges. Absolute and average {min; max} are obtained as described in Table 4.

MN property	Unit	Absolute exp {min;max}	Average exp {min; max}	$\boldsymbol{q_A^E}$	Reference studies	$\boldsymbol{q_A^T}$	$\boldsymbol{\frac{q_A^E}{q_A^T}}$	Theoretical range
$\boldsymbol{R}$	$M\Omega$	$\{0.2; 8.1\}$	$\{0.4; 4.0\}$	10.9	(Kernell, 1966; Burke, 1968; Burke & Ten Bruggencate, 1971; Barrett & Crill, 1974; Gustafsson, B., 1979; Kernell & Zwaagstra, 1981; Fleshman et al., 1981; Burke et al., 1982; Ulfhake, B. & Kellerth, 1984; Gustafsson & Pinter, 1984a; Zengel et al., 1985; Foehring et al., 1986; Munson et al., 1986; Foehring et al., 1987; Sasaki, 1991; Krawitz et al., 2001)	8.4	1.3	$[0.5; 4.0]$
$\boldsymbol{C}$	nF	$\{2.2; 8.5\}$	$\{2.2; 8.5\}$	3.9	(Gustafsson & Pinter, 1984a; Gustafsson & Pinter, 1985)	2.3	1.6	$[3.2; 7.5]$
$\boldsymbol{\tau}$	ms	$\{2.0; 14.2\}$	$\{2.9; 10.2\}$	3.5	(Burke & Ten Bruggencate, 1971; Barrett & Crill, 1974; Gustafsson, B., 1979; Ulfhake, B. & Kellerth, 1984; Gustafsson & Pinter, 1984a; Gustafsson & Pinter, 1985; Sasaki, 1991)	3.7	0.9	$[2.8; 10.3]$
$\boldsymbol{I_{th}}$	nA	$\{1.7; 52.7\}$	$\{2.3; 36.6\}$	16.3	(Fleshman et al., 1981; Kernell & Monster, 1981; Ulfhake, B. & Kellerth, 1984; Gustafsson & Pinter, 1984b; Zengel et al., 1985; Foehring et al., 1986; Munson et al., 1986; Foehring et al., 1987; Krawitz et al., 2001)	9.1	1.8	$[3.9; 35.0]$
$\boldsymbol{AHP}$	ms	$\{10.6; 266.6\}$	$\{44.2; 158.7\}$	4.1	(Eccles et al., 1957; Gustafsson, B., 1979; Dum & Kennedy, 1980; Zwaagstra, B. & Kernell, 1980; Ulfhake, B. & Kellerth, 1984; Gustafsson & Pinter, 1984a; Zengel et al., 1985; Foehring et al., 1987; Sasaki, 1991)	3.8	1.1	$[42.6; 160.2]$
$\boldsymbol{ACV}$	$m \cdot s^{-1}$	$\{51.1; 127.2\}$	$\{65.3; 114.8\}$	1.8	(Eccles et al., 1957; McPhedran et al., 1965; Kernell, 1966; Appelberg & Emonet-Dénand, 1967; Burke, 1968; Barrett & Crill, 1974; Proske & Waite, 1974; Bagust, 1974; Stephens & Stuart, 1975; Cullheim, 1978; Dum & Kennedy, 1980; Zwaagstra, B. & Kernell, 1980; Kernell & Zwaagstra, 1981; Fleshman et al., 1981; Glenn & Dement, 1981; Burke et al., 1982; Gustafsson & Pinter, 1984a; Zengel et al., 1985; Foehring et al., 1986; Foehring et al., 1987)	2.3	0.8	$[63.5; 116.6]$

The normalized relationships were finally scaled using the theoretical ranges reported in the last column of Table 5. Taking the $\{I_{th}; R\}$ pair as example, as $I_{th} = 1.4 \cdot 10^3 \cdot R^{-1}$ (normalized relationship derived previously and provided in Supplementary Material), $R \in [0.5; 4.0] \cdot 10^6 \Omega$ and

$I_{th} \in [3.9; 35.0] \cdot 10^{-9} A$ (Table 5), it was directly obtained from the Methods that $I_{th} = \frac{2.7 \cdot 10^{-2}}{R} = \frac{\Delta V^{th}}{I^{th}}$ in SI base units. A similar approach yielded the mathematical relationships reported in Table 6 between all MN electrophysiological and morphometric properties $ACV, AHP, R, I_{th}, C, \tau$ and S_{MN}. All constants and relationships are given in SI base units. The specific capacitance C_m and the membrane voltage threshold ΔV_{th} were found to be constant among MNs, a property discussed in the Discussion section.

<u>Specific resistance R_m</u>

A specific membrane input resistance is generally defined in the literature (Barrett & Crill, 1974; Burke et al., 1982; Kernell, 2006) as the surface input resistance $R = \frac{R_m}{S_{neuron}}$. According to the relationships in Table 6, we obtain $R = \frac{R_m}{S_{neuron}} = \frac{1.7 \cdot 10^{-10}}{S_{neuron}^{2.4}}$, which yields $R_m = \frac{1.7 \cdot 10^{-10}}{S_{neuron}^{1.4}}$. This finding is consistent with the conclusions from Barrett & Crill (1974), who reported a weak but significant linear relationship between R_m and $1/S_{MN}$. Also, $R_m = \frac{1.7 \cdot 10^{-10}}{S_{MN}^{1.4}}$ yields $R_m = 4.1 \cdot AHP^{0.9}$ from the relationships in Table 6, which is consistent with the indirect conclusion of a positive correlation between R_m and AHP in Gustafsson & Pinter (1984b). Finally, considering that $q_S^E = 2.4$ and $S_{neuron} \in [0.18; 0.44]\ mm^2$ (Table 4), $R_m = \frac{1.7 \cdot 10^{-10}}{S_{MN}^{1.4}}$ yields that R_m varies over the q_A^E =3.5-fold theoretical range $[0.21; 0.73]\ \Omega \cdot m^2$. This is both consistent with the $q_A^E = 3.2$-fold range and the $\left[A_{min}^E;\ A_{max}^E\right] = [0.16; 0.62]\ \Omega \cdot m^2$ mean range previously speculated in the literature (Albuquerque & Thesleff, 1968; Barrett & Crill, 1974; Burke et al., 1982; Gustafsson & Pinter, 1984a; Kernell & Zwaagstra, 1989). The MN property R_m was therefore added to Table 6.

Table 6. Mathematical empirical cat relationships between the MN properties $S_{neuron}, D_{soma}, R, R_m, C, \tau, I^{th}$, AHP and ACV. Each column provides the relationships between one and the nine other MN properties. If one property is known, the complete MN profile can be reconstructed by using the pertinent line in this table. All constants and properties are provided in SI base units (meters, seconds, ohms, farads and ampers). These relationships were obtained for alpha-MNs innervating the hindlimbs of adult cats in vivo.

	$S_{neuron}[m^2]$	$D_{soma}[m]$	$R[\Omega]$	$R_m[\Omega \cdot m^2]$	$C[F]$	$\tau[s]$	$I_{th}[A]$	$AHP[s]$	$ACV[m \cdot s^{-1}]$
$S_{neuron}[m^2]$		$D_{soma} = 1.8 \cdot 10^2 \cdot S_{neuron}$	$R = \frac{1.7 \cdot 10^{-10}}{S_{neuron}^{2.4}}$	$R_m = \frac{1.7 \cdot 10^{-10}}{S_{neuron}^{1.4}}$	$C = 1.0 \cdot 10^{-2} \cdot S_{neuron}$	$\tau = \frac{1.0 \cdot 10^{-12}}{S_{neuron}^{1.5}}$	$I_{th} = 3.8 \cdot 10^8 \cdot S_{neuron}^{2.5}$	$AHP = \frac{1.0 \cdot 10^{-11}}{S_{neuron}^{1.5}}$	$ACV = 3.0 \cdot 10^6 \cdot S_{neuron}^{0.7}$
$D_{soma}[m]$	$S_{neuron} = 5.5 \cdot 10^{-3} \cdot D_{soma}$		$R = \frac{5.1 \cdot 10^{-5}}{D_{soma}^{2.4}}$	$R_m = \frac{2.8 \cdot 10^{-7}}{D_{soma}^{1.4}}$	$C = 6.7 \cdot 10^{-5} \cdot D_{soma}$	$\tau = \frac{2.3 \cdot 10^{-9}}{D_{soma}^{1.5}}$	$I_{th} = 7.8 \cdot 10^2 \cdot D_{soma}^{2.5}$	$AHP = \frac{2.7 \cdot 10^{-8}}{D_{soma}^{1.5}}$	$ACV = 8.1 \cdot 10^4 \cdot D_{soma}^{0.7}$
$R[\Omega]$	$S_{neuron} = \frac{9.5 \cdot 10^{-5}}{R^{0.4}}$	$D_{soma} = \frac{1.7 \cdot 10^{-2}}{R^{0.4}}$		$R_m = 9.5 \cdot 10^{-5} \cdot R^{0.6}$	$C = \frac{1.3 \cdot 10^{-6}}{R^{0.4}}$	$\tau = 9.6 \cdot 10^{-7} \cdot R^{0.6}$	$I_{th} = \frac{2.7 \cdot 10^{-2}}{R}$	$AHP = 1.3 \cdot 10^{-5} \cdot R^{0.6}$	$ACV = \frac{4.9 \cdot 10^3}{R^{0.3}}$
$R_m[\Omega \cdot m^2]$	$S_{neuron} = \frac{1.5 \cdot 10^{-7}}{R_m^{0.7}}$	$D_{soma} = \frac{2.6 \cdot 10^{-5}}{R_m^{0.7}}$	$R = 6.8 \cdot 10^6 \cdot R_m^{1.7}$		$C = \frac{2.6 \cdot 10^{-9}}{R_m^{0.7}}$	$\tau = 1.4 \cdot 10^{-2} \cdot R_m$	$I_{th} = \frac{2.2 \cdot 10^{-9}}{R_m^{1.8}}$	$AHP = 2.2 \cdot 10^{-1} \cdot R_m^{1.1}$	$ACV = \frac{5.4 \cdot 10^1}{R_m^{0.5}}$
$C[F]$	$S_{neuron} = 1.2 \cdot 10^2 \cdot C$	$D_{soma} = 2.1 \cdot 10^4 \cdot C$	$R = \frac{1.5 \cdot 10^{-15}}{C^{2.5}}$	$R_m = \frac{1.8 \cdot 10^{-13}}{C^{1.5}}$		$\tau = \frac{8.6 \cdot 10^{-16}}{C^{1.5}}$	$I_{th} = 6.5 \cdot 10^{13} \cdot C^{2.6}$	$AHP = \frac{7.7 \cdot 10^{-15}}{C^{1.6}}$	$ACV = 8.2 \cdot 10^7 \cdot C^{0.7}$
$\tau[s]$	$S_{neuron} = \frac{8.4 \cdot 10^{-9}}{\tau^{0.7}}$	$D_{soma} = \frac{1.5 \cdot 10^{-6}}{\tau^{0.7}}$	$R = 7.1 \cdot 10^9 \cdot \tau^{1.6}$	$R_m = 6.0 \cdot 10^1 \cdot \tau$	$C = \frac{1.6 \cdot 10^{-10}}{\tau^{0.6}}$		$I_{th} = \frac{1.6 \cdot 10^{-12}}{\tau^{1.7}}$	$AHP = 1.7 \cdot 10^1 \cdot \tau$	$ACV = \frac{7.5}{\tau^{0.5}}$
$I_{th}[A]$	$S_{neuron} = 4.0 \cdot 10^{-4} \cdot I_{th}^{0.4}$	$D_{soma} = 7.1 \cdot 10^{-2} \cdot I_{th}^{0.4}$	$R = \frac{3.1 \cdot 10^{-2}}{I_{th}}$	$R_m = \frac{1.2 \cdot 10^{-5}}{I_{th}^{0.6}}$	$C = 5.3 \cdot 10^{-6} \cdot I_{th}^{0.4}$	$\tau = \frac{1.2 \cdot 10^{-7}}{I_{th}^{0.6}}$		$AHP = \frac{1.5 \cdot 10^{-6}}{I_{th}^{0.6}}$	$ACV = 1.3 \cdot 10^4 \cdot I_{th}^{0.3}$
$AHP[s]$	$S_{neuron} = \frac{5.5 \cdot 10^{-8}}{AHP^{0.7}}$	$D_{soma} = \frac{9.8 \cdot 10^{-6}}{AHP^{0.7}}$	$R = 7.5 \cdot 10^7 \cdot AHP^{1.6}$	$R_m = 4.1 \cdot AHP^{0.9}$	$C = \frac{1.0 * 10^{-9}}{AHP^{0.6}}$	$\tau = 6.2 \cdot 10^{-2} \cdot AHP$	$I_{th} = \frac{1.8 * 10^{-10}}{AHP^{1.7}}$		$ACV = \frac{2.7 \cdot 10^1}{AHP^{0.5}}$
$ACV[m \cdot s^{-1}]$	$S_{neuron} = 4.6 \cdot 10^{-10} \cdot ACV^{1.4}$	$D_{soma} = 8.3 \cdot 10^{-8} \cdot ACV^{1.4}$	$R = \frac{8.3 \cdot 10^{12}}{ACV^{3.5}}$	$R_m = \frac{3.8 \cdot 10^3}{ACV^{2.1}}$	$C = 1.0 \cdot 10^{-11} \cdot ACV^{1.4}$	$\tau = \frac{7.4 \cdot 10^1}{ACV^{2.1}}$	$I_{th} = 1.1 \cdot 10^{-15} \cdot ACV^{3.6}$	$AHP = \frac{1.4 \cdot 10^3}{ACV^{2.2}}$	

553 Predicting correlations between MN properties

554 This study also predicts the correlations between MN properties that were either never reported in
555 past review studies, such as the positive $S_{MN} - \tau$ relationship, or never concurrently measured in the
556 literature, as displayed in Figure 2B. Such unknown relationships were indirectly extracted from the
557 combination of known relationships (Table 3) and typical ranges of values obtained from the literature
558 for these properties. Due to the prior validation of the relationships in Table 6, these findings are
559 reliable as indirectly consistent with the literature data processed in this study and provide new
560 insights on the size-dependency of the MN recruitment mechanisms.

561 Extrapolation to rats and mice

562 It was assessed whether the scaled relationships obtained from cat data and reported in Table 6 could
563 be successfully applied to rat and mouse data. A global $\{I_{th}; R\}$ dataset was obtained from 5 studies
564 focusing on rats reported in Table 7, while four mice studies reported in Table 7 provided processable
565 data for the pairs $\{I_{th}; R\}$, $\{\tau; R\}$ and $\{C; R\}$. Figure 7 reports the global datasets for all 4 pairs of
566 properties and the predictions obtained with the cat relationships reported in Table 6. As displayed in
567 Table 7, r^2_{pred} and r^2_{exp} values were close for all 4 datasets, with a maximum 12.5% difference for
568 $\{\tau; R\}$ in mice. $nRMSE$ values remained low in both rat and mouse $\{I_{th}; R\}$ datasets, while being
569 substantially higher in both $\{\tau; R\}$ and $\{C; R\}$ datasets in mice because of an inter-species-specific
570 offset in the relationships.

571 **Table 7. Validation of the cat relationships (Table 6) against rat and mouse data**. nME: normalized maximum
572 error. nRMSE: normalized root-mean-square error. r^2_{pred}: coefficient of determination between experimental
573 and predicted quantities. r^2_{exp} : coefficient of determination of the power trendline directly fitted to the
574 experimental data.

Animal	Dataset	Reference studies	nME (%)	$nRMSE$ (%)	r^2_{pred}	r^2_{exp}
Rat	$\{I_{th}; R\}$	(Gardiner, 1993; Bakels & Kernell, 1993; Lee & Heckman, 1998; Button et al., 2008; Turkin et al., 2010; Krutki et al., 2015)	591	16	0.53	0.54
Mouse	$\{I_{th}; R\}$	(Delestrée et al., 2014; De Lourdes Martínez-Silva et al., 2018; Huh et al., 2021)	621	17	0.37	0.41
	$\{\tau; R\}$	(Manuel et al., 2009b)	1183	155	0.35	0.40
	$\{C; R\}$	(Manuel et al., 2009b)	1802	87	0.38	0.38

575

576

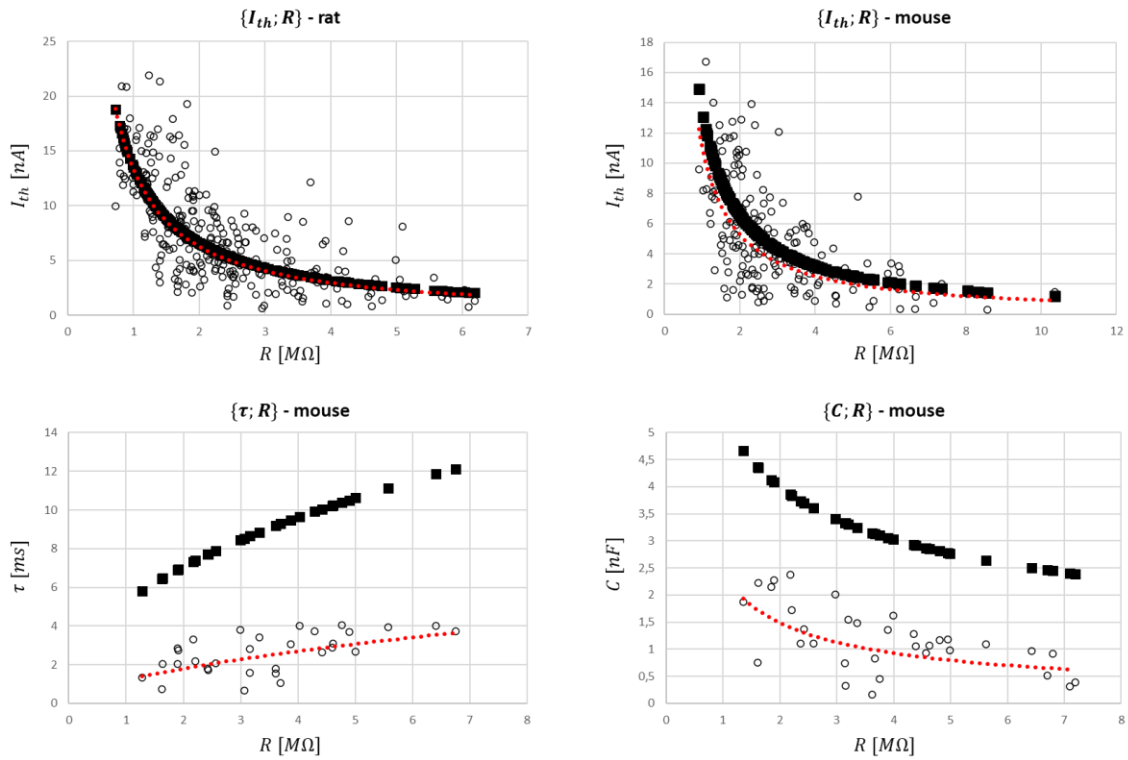

Figure 7. Global datasets for rat and mouse species and predictions of the MN properties with the cat mathematical relationships (Table 6). They were obtained from the 5 studies reporting data on rats and the 4 studies presenting data on mice reported in Table 7 that measured the $\{I_{th}; R\}$, $\{\tau; R\}$ and $\{C; R\}$ pairs of MN electrophysiological properties. I_{th}, R, τ, C are given in $nA, M\Omega, ms$ and nF respectively. The experimental data (○ symbol) is fitted with a power trendline (red dotted curve) and compared to the predicted quantities obtained with the scaled cat relationships in Table 6 (■ symbol).

Relationships between MN and mU properties

As shown in Figure 2A, eight pairs of one MN and one mU property were investigated in 14 studies in the literature in cats and rats. As remarked by Heckman & Enoka (2012) and Manuel et al. (2019), most recent studies were performed on mice, while most dated were dominantly performed on cats. One study on the rat gastrocnemius muscle (Kanda & Hashizume, 1992) indicated no correlation between IR and CV. However, after removing from the dataset 2 outliers that fell outside two standard deviations of the mean IR data, a statistically significant correlation ($p < 0.05$) between IR and CV was successfully fitted with a power trendline ($r^2 = 0.43$). Eight studies, dominantly focusing on the cat soleus and medial gastrocnemius muscles, found a strong correlation between F^{tet} and CV, while one study showed a significant correlation for the pair $\{F^{tet}; R\}$ in both the cat tibialis anterior and extensor digitorum longus muscles. One study (Burke *et al.*, 1982) on the cat soleus, medial and lateral gastrocnemius muscles inferred a statistically significant correlation for $\{F^{tet}; S_{MN}\}$. In mice, both R and I_{th} were significantly related to muscle tetanic and twitch forces. As F^{tet}, F^{tw} and IR are reliable

indices of S_{mU} as discussed in the Methods, the MN size-dependent relationships in Table 3 return eight $S_{mU} = k \cdot S_{MN}^{c}$ relationships between mU and MN properties (Table 8). A 2.8-fold range in positive c-values $c \in [2.4; 6.6]$ (mean 3.8 ± 1.5 s.d.) was obtained between studies. This result infers than mU and MN size are positively related in cats, mice and potentially in rats.

Table 8. Fitted experimental data of pairs of one mU and one MN property and subsequent $\boldsymbol{S_{mU} \propto S_{MN}^{c}}$ relationships. The r^2, p-value and the equation $A \propto B^c$ of the trendlines are reported for each pair of properties. In the last column, prior knowledge is used to derive $S_{mU} \propto S_{MN}^{c}$ relationships.

Species	$\boldsymbol{A = k \cdot B^c}$ (fitted relationships)					$\boldsymbol{S_{mU} = k \cdot S_{MN}^{c}}$ (final relationships)
	Relationship	c	r^2	p-value	Reference studies	c
Rat	$IR = k \cdot CV^c$	3.4	0.45	$6 \cdot 10^{-3}$	(Kanda & Hashizume, 1992)	2.4
Cat	$F^{tw} = k \cdot CV^c$	9.4	0.43	$p < 10^{-5}$	(Knott et al., 1971)	6.6
	$F^{tet} = k \cdot CV^c$	7.2	0.37	$p < 10^{-5}$	(McPhedran et al., 1965; Wuerker et al., 1965; Appelberg & Emonet-Dénand, 1967; Proske & Waite, 1974; Bagust, 1974; Jami & Petit, 1975; Stephens & Stuart, 1975; Burke et al., 1982; Emonet-Dénand et al., 1988)	5.0
	$F^{tet} = k \cdot R^c$	-1.3	0.27	$6 \cdot 10^{-5}$	(Dum & Kennedy, 1980)	3.2
	$F^{tet} = k \cdot S_{MN}^{c}$	2.0	0.21	$2 \cdot 10^{-2}$	(Burke *et al.*, 1982)	2.0
Mouse	$F^{tw} = k \cdot R^c$	-2.1	0.42	$p < 10^{-5}$	(Manuel & Heckman, 2011; De Lourdes Martínez-Silva et al., 2018)	5.1
	$F^{tw} = k \cdot I_{th}^{c}$	1.3	0.64	$2 \cdot 10^{-4}$	(Manuel & Heckman, 2011)	3.3
	$F^{tet} = k \cdot I_{th}^{c}$	1.0	0.80	$6 \cdot 10^{-2}$	(Manuel & Heckman, 2011)	2.5
Mean ±sd						3.8 ± 1.5

Discussion

We processed the data (Figure 3) from previous cat experimental studies to extract mathematical relationships (Table 6) between several MN electrophysiological properties and MN size (Table 1). First, this allowed us to demonstrate that all investigated MN properties are predicted by MN size (Table 3, Figure 4, Figure 5) and that electrophysiological properties at the level of individual MNs are interrelated. Second, we established (Table 6) and validated (Figure 6) mathematical relationships linking all the pairs of MN properties, providing the first mathematical framework for building virtual MN pools of MN-specific morphometric and electrophysiological properties that are consistent with published experimental cat data *in vivo*. The mathematical relationships reported in Table 6 are a new important tool for neuroscientists, experimenters, and modelers, as discussed in the following.

Advanced insights in MN neurophysiology

The findings in Table 3, Figure 4, Figure 5 and Table 6 advance our knowledge on the neural electrophysiology beyond the experimental data available in the literature and provide a quantified demonstration to considerations from previous literature reviews, either drawn from direct but isolated measurements or speculated. For example, Binder et al. (1996) concluded that the AHP duration was inversely related to MN size S_{MN} based on measures of a single experimental study. Conversely, the size-dependencies of R and I_{th} were qualitatively assumed by Powers & Binder (2001) from the equations obtained from a variant of Rall's model of MN membrane equivalent electrical circuit (Rall, 1957; Rall, 1959; Rall, 1960), and not from experimental data. The negative correlation between S_{MN} and R was predicted by Binder et al. (1996) from the findings of Henneman's studies on the correlation between extracellular spike amplitude and S_{MN} (Henneman, 1957; Henneman et al., 1965a). The fact that R defines the MN rheobase and thus dictates the size order of MN recruitment was similarly justified in Binder et al. (1996) and Powers & Binder (2001) from a combination of Henneman's findings and Rall's model equations. Moreover, all previous papers used the debated association between motor unit type and S_{MN} , mainly obtained from measures in the cat gastrocnemius muscle (Fleshman et al., 1981; Burke et al., 1982; Zengel et al., 1985; Bakels & Kernell, 1993), to indirectly speculate on correlations between S_{MN} and AHP (Heckman & Enoka, 2012), R (Powers & Binder, 2001; Heckman & Enoka, 2012), R_m (Binder et al., 1996; Powers & Binder, 2001) or I_{th} (Binder et al., 1996). Finally, we found a single paper that inferred a positive correlation between S_{MN} and C (Heckman & Enoka, 2012) but without reference to direct experimental results.

Some relationships in Table 6 also advance our general understanding of the MN neurophysiology because they were inferred for pairs of MN properties that were never concurrently measured in experiments (Figure 2B) by crossmatching other relationships involving these properties. $I_{th} = 3.8 \cdot$

640 $10^8 \cdot S_{neuron}^{2.5}$ or $\tau = \frac{8.6 \cdot 10^{-16}}{C^{1.5}}$ (Table 6) for instance confirm the respective speculations that the larger
641 the MN, the larger its current threshold and the larger the MN membrane capacitance, the lower its
642 time constant for eliciting action potentials. With the same approach, the relationships in Table 6
643 predict the behavior of MN properties that cannot be measured in experiments, such as the MN
644 specific capacitance and input resistance. The extrapolation of the experimental data in Figure 3 with
645 continuous trendlines estimates possible values of electrophysiological properties for the smallest and
646 largest MNs of the MN pool, which are suspected not to be systematically identified in the sample of
647 small size provided in the available experimental studies, and may provide a more realistic picture of
648 the typical ranges of property values in a complete MN pool.

649 **Relevance for other mammals**

650 It is demonstrated in Figure 7 and with the calculation of the r^2 values in Table 7 that the mathematical
651 equations in Table 6 obtained from cat data adequately predict the normalized associations between
652 pairs of MN properties in rats and mice. However, the scaling factor K applied to the intercept k_e to
653 scale the normalized relationships $A = K \cdot k_e \cdot B^e$ is species-specific, being for example around 3
654 times smaller in mice than in cat for the $\{\tau; R\}$ and $\{C; R\}$ pairs (Figure 7) and explaining the large
655 $nRMSE$ values in these cases. Absolute values of the $\{I_{th}; R\}$ pair were nevertheless accurately
656 predicted in both rats and mice from the cat relationships, as explained by the larger values of R which
657 counterbalances the respectively lower I_{th} values in mice and rats than in cats (Manuel et al., 2019;
658 Highlander et al., 2020). These findings advance our understanding of the systematic inter-
659 mammalian-species variations in MN properties. While the mathematical equations in Table 6 are
660 specific to cats, the normalized equations in Supplementary Material can be scaled with species-
661 specific data if investigating other mammals, and may provide a tool to neuroscientists to estimate the
662 MN property values that cannot be measured in humans *in vivo*.

663 **Relevance for MN modelling**

664 The empirical equations in Table 6 provide a mathematical framework that supports the common
665 approach of modelling the MN membrane behaviour with an equivalent resistance-capacitance
666 electrical circuit as variants of Rall's cable model (Rall, 1957; Rall, 1959; Rall, 1960). The relationship
667 $C = 1.0 \cdot 10^{-2} \cdot S_{MN}^{1.0}$ reported in Table 6 validates the definition $C = C_m \cdot S_{MN}$, as well as emphasizing
668 that the specific capacitance C_m per unit area is constant among the MN pool, and indirectly yields,
669 from typical ranges of C and S_{MN} in the literature, the relation $C_m = 1.0 \cdot 10^{-2} F \cdot m^{-2}$, which is highly
670 consistent with the typical values reported in the literature (Lux & Pollen, 1966; Albuquerque &
671 Thesleff, 1968; Barrett & Crill, 1974; Adrian & Hodgkin, 1975; Sukhorukov et al., 1993; Major et al.,

672 1994; Solsona et al., 1998; Thurbon et al., 1998; Gentet et al., 2000). Similarly, the empirical
673 relationship $I_{th} = \frac{2.7 \cdot 10^{-2}}{R^{1.0}}$ (Table 6) yields $\Delta V_{th} = 27mV$, consistently with typical reported values
674 (Brock et al., 1952; Eccles et al., 1958), despite uncertainties in the value of the membrane resting
675 potential (Heckman & Enoka, 2012). This supports the conclusions that the relative voltage threshold
676 ΔV_{th} is constant within the MN pool (Coombs et al., 1955; Gustafsson & Pinter, 1984a; Gustafsson &
677 Pinter, 1984b; Powers & Binder, 2001), and that Ohm's law is followed in MNs (Glenn & Dement, 1981;
678 Spruston & Johnston, 1992; Kernell, 2006). Also, no correlation between $\frac{\Delta V_{th}}{R \cdot I_{th}}$ and C is reported in
679 Table 6, consistent with measurements performed by Gustafsson & Pinter (1984b), substantiating that
680 the dynamics of MN recruitment dominantly rely on R, I^{th} and ΔV_{th} (Heckman & Enoka, 2012). Finally,
681 the findings $R = 7.1 \cdot 10^{9} \cdot \tau^{1.6}, C = 1.6 \cdot 10^{-10} \cdot \frac{1}{\tau^{0.6}}$ and $R_m = 6.0 \cdot 10^{1} \cdot \tau$, $C_m = 1.0 \cdot 10^{-2} F \cdot m^{-2}$
682 in Table 6 yield $R \cdot C = 1.1 \cdot \tau$ and $R_m \cdot C_m = 0.6 \cdot \tau$, which is consistent with the classic empirical
683 relationship $\tau = RC = R_m C_m$ (Gustafsson & Pinter, 1984a; Zengel et al., 1985).

684 With the validated relationships in Table 6, modelers can therefore tune the physiological parameters
685 of advanced models of MN membrane equivalent electrical circuit, such as the leaky fire-and-integrate
686 model, that provide more detailed representations of the neural behaviour than simpler approaches
687 (Fuglevand 1993) where the MN firing frequency is modelled as a linear function of the synaptic input.
688 The relationships in Table 6 make it possible to describe pools of MNs displaying a continuous
689 distribution of realistic MN profiles of MN-specific electrophysiological properties. This latter approach
690 involving advanced and realistic MN models may lead to more accurate predictions of the neural
691 behaviour of mammalian MN pools, the interpretation of which will also be facilitated, and which will
692 accelerate our understanding of the neuromechanical interplay that underlines motor control in
693 mammalian voluntary motion.

694 **Relevance for *in vivo* experiments**

695 The mathematical relationships in Table 6 can support future experimental investigations performed
696 on spinal MNs in adult mammals *in vivo* by completing experimental datasets for which properties that
697 are difficult to measure were not obtained, such as the MN membrane capacitance. Experimenters
698 can therefore choose to reduce the workload of measuring all the MN properties in Table 1 to favour
699 the identification of a maximum number of MNs and obtain extensive datasets describing larger MN
700 populations that provide an informative window on the continuous distribution of MN properties in a
701 MN pool. The unknown electrophysiological MN properties, typically obtained *in vivo*, of cadaveric
702 specimens can also be estimated with the size-related relationships in Table 6 from in vitro
703 measurements of the somal diameter D_{soma}in a slice preparation of the spinal cord. The mathematical

704 relationships in Table 6 describe the experimental data published in the literature and provide a
705 convenient metric for experimenters to compare their measurements to previous findings.

706 **Henneman's size principle of motor unit recruitment**

707 Table 8 reports statistically significant power relationships of positive power values between MN and
708 mU indices of size. These results substantiate the concept that S_{MN} and S_{mU} are positively correlated
709 in a motor unit (MU) pool and that large MNs innervate large mUs (Henneman, 1981; Heckman &
710 Enoka, 2012), a statement that has never been demonstrated from the concurrent direct
711 measurement of S_{MN} and S_{mU}. Besides, considering the positive $I_{th} - S_{MN}$ correlation (Table 6), and
712 that the mU force recruitment threshold F^{th} is positively correlated to F^{tet} (Heckman & Enoka, 2012)
713 and thus to S_{mU} (Table 2), larger MUs have both larger current and force recruitment thresholds I_{th}
714 and F^{th} than relatively smaller MUs, which are thus recruited first, consistently with the Henneman's
715 size principle of MU recruitment (Henneman, 1957; Wuerker et al., 1965; Henneman et al., 1965a;
716 Henneman et al., 1965b; Henneman et al., 1974; Henneman, 1981; Henneman, 1985). The
717 terminologies 'small MU', 'low-force MU' and 'low-threshold MU' are thus equivalent. Henneman's
718 size principle thus relies on the amplitude of the MN membrane resistance (Binder et al., 1996; Powers
719 & Binder, 2001; Heckman & Enoka, 2012). Finally, the relationships $S_{MN} \propto CV^{1.4} \propto \tau^{-0.7} \propto AHP^{-0.7}$
720 (Table 6) suggest that high-threshold MUs rely on relatively faster MN dynamics, which might partially
721 explain why large MNs can attain relatively larger firing rates than low-thresholds MNs.

722 It has been repeatedly attempted to extend Henneman's size principle and the correlations between
723 the MU properties in Table 1 to the concept of 'MU type' (Burke & Ten Bruggencate, 1971; Burke,
724 1981; Bakels & Kernell, 1993; Powers & Binder, 2001). While a significant association between 'MU
725 type' and indices of MU size has been observed in some animal (Fleshman et al., 1981; Burke et al.,
726 1982; Zengel et al., 1985) and a few human (Milner-Brown et al., 1973; Stephens & Usherwood, 1977;
727 Garnett et al., 1979; Andreassen & Arendt-Nielsen, 1987) studies, it has however not been observed
728 in other animal studies ((Bigland-Ritchie et al., 1998) for a review) and in the majority of human
729 investigations (Sica & McComas, 1971; Goldberg & Derfler, 1977; Yemm, 1977; Young & Mayer, 1982;
730 Thomas et al., 1990; Nordstrom & Miles, 1990; Elek et al., 1992; Macefield et al., 1996; Cutsem et al.,
731 1997; Mateika et al., 1998; Fuglevand et al., 1999; Keen & Fuglevand, 2004). Moreover, the reliability
732 of these results is weakened by the strong limitations of the typical MU type identification protocols.
733 Sag experiments are irrelevant in humans (Buchthal & Schmalbruch, 1970; Thomas et al., 1991; Bakels
734 & Kernell, 1993; Macefield et al., 1996; Bigland-Ritchie et al., 1998; Fuglevand et al., 1999), and lack
735 consistency with other identification methods (Nordstrom & Miles, 1990). MU type identification by
736 twitch contraction time measurements is limited by the strong sources of inaccuracy involved in the

transcutaneous stimulation, intramuscular microstimulation, intraneural stimulation, and spike-triggered averaging techniques (Taylor et al., 2002; Keen & Fuglevand, 2004; McNulty & Macefield, 2005; Negro et al., 2014; Dideriksen & Negro, 2018). Finally, as muscle fibres show a continuous distribution of contractile properties among the MU pool, some MUs fail to be categorized in discrete MU types in some animal studies by histochemical approaches (Reinking et al., 1975; Totosy de Zepetnek et al., 1992). Owing to these conflicting results and technical limitations, MU type may not be related to MN size and the basis for MU recruitment during voluntary contractions (McNulty & Macefield, 2005; Duchateau & Enoka, 2011).

Limitations

The mathematical relationships derived Table 6 and the conclusions drawn in the Discussion present some limitations, which were partly discussed in the Methods and Result sections and are summarised here. A first limitation is related to the normalization of all datasets to the highest measured value retrieved in each study; this approach is only valid if the experimental studies identified the same largest MN relatively to the MN populations under investigation. This cannot be verified and is unlikely, considering the small MN populations investigated in most selected studies. A second limitation is due to the limited processable experimental data available in the literature, especially in rats and mice, as also discussed by Heckman & Enoka (2012). Therefore, some pairs of MN properties were investigated in only one study, especially those involving C, preventing inter-study comparisons. For the same reason, measurements obtained from MNs innervating different muscles from cats of different sex were merged into unique datasets, implicitly assuming no sex- and muscle-specific distributions of MN properties within the MN pools. Besides, only MNs innervating the hindlimbs were investigated. The extrapolation of the relationships in Table 6 to rat and mouse species could only be assessed against a small set of studies and for three associations only. Finally, the conclusions on the associations between S_{mU} and S_{MN} relied on few studies providing few measurements, due to the challenging experimental protocols and the considerable amount of work required to measure both MN and mU properties in single MUs. Thirdly, the available data comes from relatively dated cat studies, as observed in Manuel et al. (2019). Thus, recent computer-assisted techniques of MN morphometric measurements were notably not applicable in those studies, yielding important sources of inaccuracies, as discussed. Therefore, the relationships involving S_{neuron} are subjected to a higher level of inaccuracy. Consequently, the mathematical relationships in Table 6 best reproduce published cat data but include the level of inaccuracies of the original experimental approaches.

Conclusion

This study provides the first empirical and algebraical proof that the MN properties ($S_{MN}, ACV, AHP, R, I_{th}, C$ and τ) are related. The derived mathematical relationships between any of these MN properties and/or S_{MN} (Table 6) accurately describe the experimental data available in the literature. This mathematical framework constitutes a convenient tool for neuroscientists, experimenters, and modelers to investigate the neurophysiology of MN pools, generate hypothesis for experimental studies aiming at investigating currently unreported relationships, support experimentations and build virtual MN profiles of inter-consistent MN-specific properties for MN modelling purposes.

References

Adrian RH, Hodgkin AL (1975) Conduction velocity and gating current in the squid giant axon. Proc. Royal Soc. 189:81-86.

Albuquerque EX, Thesleff S (1968) A comparative study of membrane properties of innervated and chronically denervated fast and slow skeletal muscles of the rat. Acta Physiol. Scand. 73:471-480.

Amendola J, Durand J (2008) Morphological differences between wild-type and transgenic superoxide dismutase 1 lumbar motoneurons in postnatal mice. Journal of comparative neurology (1911) 511:329-341.

Andreassen S, Arendt-Nielsen L (1987) Muscle fibre conduction velocity in motor units of the human anterior tibial muscle: A new size principle parameter. J. Physiol. 391:561-571.

Ankit, R. (2020) WebPlotDigitizer. **4.4** https://automeris.io/WebPlotDigitizer.

Appelberg B, Emonet-Dénand F (1967) Motor units of the first superficial lumbrical muscle of the cat. J. Neurophysiol. 30:154-160.

Bagust J (1974) Relationships between motor nerve conduction velocities and motor unit contraction characteristics in a slow twitch muscle of the cat. J. Physiol. 238:269-278.

Bakels R, Kernell D (1993) Matching between motoneurone and muscle unit properties in rat medial gastrocnemius. J. Physiol. 463:307-324.

Barrett JN, Crill WE (1974) Specific membrane properties of cat motoneurones. J. Physiol. 239:301-324.

Bigland-Ritchie B, Fuglevand AJ, Thomas CK (1998) Contractile properties of human motor units: Is man a cat? The Neuroscientist 4:240-249.

Binder, M. D., Heckman, C. J. & Powers, R. K. (1996) The physiological control of motoneuron activity. In Rowell LB, S. J. (ed), *Handbook of Physiology: Exercise, Regulation and Integration of Multiple Systems.* New York: Oxford Univ Press, pp. 3-53.

Bodine SC, Roy RR, Eldred E, Edgerton VR (1987) Maximal force as a function of anatomical features of motor units in the cat tibialis anterior. J. Neurophysiol. 57:1730-1745.

Brandenburg, J. E.,Fogarty, M.J.,Brown, A.D.,Sieck, G.C.(2020) Phrenic motor neuron loss in an animal model of early onset hypertonia. Journal of Neurophysiology, **123**, 1682.

Brandenburg, J. E.,Gransee, H.M.,Fogarty, M.J.,Sieck, G.C.(2018) Differences in lumbar motor neuron pruning in an animal model of early onset spasticity. Journal of Neurophysiology, **120**, 601.

Brock LG, Coombs JS, Eccles JC (1952) The recording of potentials from motoneurones with an intracellular electrode. J.Physiol.(Lond.) 117:431-460.

Buchthal F, Schmalbruch H (1970) Contraction times and fibre types in intact human muscle. Acta Physiol. Scand. 79:435-452.

811 Burke RE, Ten Bruggencate G (1971) Electrotonic characteristics of alpha motoneurones of varying
812 size. J. Physiol. 212:1-20.

813 Burke RE, Dum RP, Fleshman JW, Glenn LL, Lev-Tov A, O'Donovan MJ, Pinter MJ (1982) An HRP study
814 of the relation between cell size and motor unit type in cat ankle extensor motoneurons. J. Comp.
815 Neurol. 209:17-28.

816 Burke RE, Tsairis P (1973) Anatomy and innervation ratios in motor units of cat gastrocnemius. J.
817 Physiol. 234:749-765.

818 Burke RE (1968) Firing patterns of gastrocnemius motor units in the decerebrate cat. J. Physiol.
819 196:631-654.

820 Burke, R. E. (1981) Motor units: Anatomy, physiology, and functional organization. In Brooks, V. B.
821 (ed), *Handbook of Physiology, the Nervous System, Motor Control.* American Physiological Society,
822 pp. 345-422.

823 Button DC, Kalmar JM, Gardiner K, Marqueste T, Zhong H, Roy RR, Edgerton VR, Gardiner PF (2008)
824 Does elimination of afferent input modify the changes in rat motoneurone properties that occur
825 following chronic spinal cord transection? The Journal of physiology 586:529-544.

826 Carp JS, Tennissen AM, Mongeluzi DL, Dudek CJ, Chen XY, Wolpaw JR (2008) An in vitro protocol for
827 recording from spinal motoneurons of adult rats. Journal of Neurophysiology 100:474-481.

828 Carrascal L, Nieto-Gonzalez JL, Torres B, Nunez-Abades P (2009) Changes in somatodendritic
829 morphometry of rat oculomotor nucleus motoneurons during postnatal development. Journal of
830 comparative neurology (1911) 514:189-202.

831 Chamberlain S, Lewis DM (1989) Contractile characteristics and innervation ratio of rat soleus motor
832 units. J. Physiol. 412:1-21.

833 Coombs JS, Eccles JC, Fatt P (1955) The electrical properties of the motoneurone membrane.
834 J.Physiol.(Lond.) 130:291-325.

835 Copray, S.,Kernell, D.(2000) Neurotrophins and trk-receptors in adult rat spinal motoneurons:
836 Differences related to cell size but not to 'slow/fast' specialization. Neuroscience Letters, **289**, 217.

837 Cullheim S, Fleshman JW, Glenn LL, Burke RE (1987) Membrane area and dendritic structure in type-
838 identified triceps surae alpha motoneurons. Journal of comparative neurology (1911) 255:68-81.

839 Cullheim S (1978) Relations between cell body size, axon diameter and axon conduction velocity of
840 cat sciatic α-motoneurons stained with horseradish peroxidase. Neurosci. Lett. 8:17-20.

841 Cutsem MV, Feiereisen P, Duchateau J, Hainaut K (1997) Mechanical properties and behaviour of
842 motor units in the tibialis anterior during voluntary contractions. Can. J. Appl. Physiol. 22:585-597.

843 De Lourdes Martínez-Silva M, Imhoff-Manuel RD, Sharma A, Heckman CJ, Shneider NA, Roselli F,
844 Zytnicki D, Manuel M (2018) Hypoexcitability precedes denervation in the large fast-contracting
845 motor units in two unrelated mouse models of ALS. ELife 7:e30955.

Deardorff AS, Romer SH, Deng Z, Bullinger KL, Nardelli P, Cope TC, Fyffe REW (2013) Expression of postsynaptic Ca2+-activated K+ (SK) channels at C-bouton synapses in mammalian lumbar - motoneurons. The Journal of physiology 591:875-897.

Delestrée, N.,Manuel, M.,Iglesias, C.,Elbasiouny, S.M.,Heckman, C.J.,Zytnicki, D.(2014) Adult spinal motoneurones are not hyperexcitable in a mouse model of inherited amyotrophic lateral sclerosis. The Journal of Physiology, **592**, 1687.

Destombes J, Horcholle-Bossavit G, Thiesson D, Jami L (1992) Alpha and gamma motoneurons in the peroneal nuclei of the cat spinal cord: An ultrastructural study. Journal of comparative neurology (1911) 317:79-90.

Dideriksen JL, Negro F (2018) Spike-triggered averaging provides inaccurate estimates of motor unit twitch properties under optimal conditions. J Electromyogr Kinesiol 43:104-110.

Dong Y, Mihalas S, Russell A, Etienne-Cummings R, Niebur E (2011) Estimating parameters of generalized integrate-and-fire neurons from the maximum likelihood of spike trains. Neural Comput. 23:2833-2867.

Donselaar Y, Kernell D, Eerbeek O (1986) Soma size and oxidative enzyme activity in normal and chronically stimulated motoneurones of the cat's spinal cord. Brain Research 385:.

Duchateau J, Enoka RM (2011) Human motor unit recordings: Origins and insight into the integrated motor system. Brain Res. 1409:42-61.

Dukkipati, S. S.,Garrett, T.L.,Elbasiouny, S.M.(2018) The vulnerability of spinal motoneurons and soma size plasticity in a mouse model of amyotrophic lateral sclerosis. J Physiol, **596**, 1723.

Dum RP, Kennedy TT (1980) Physiological and histochemical characteristics of motor units in cat tibialis anterior and extensor digitorum longus muscles. J. Neurophysiol. 43:1615-1630.

Eccles JC, Libet B, Young RR (1958) The behaviour of chromatolysed motoneurones studied by intracellular recording. J.Physiol.(Lond.) 143:11-40.

Eccles JC, Eccles RM, Lundberg A (1957) Durations of after-hyperpolarization of motoneurones supplying fast and slow muscles. Nature 179:866-868.

Elek JM, Kossev A, Dengler R, Schubert M, Wohlfahrt K, Wolf W (1992) Parameters of human motor unit twitches obtained by intramuscular microstimulation. Neuromuscul. Disord. 2:261-267.

Emonet-Dénand F, Hunt CC, Petit J, Pollin B (1988) Proportion of fatigue-resistant motor units in hindlimb muscles of cat and their relation to axonal conduction velocity. J. Physiol. 400:135-158.

Enoka RM (1995) Morphological features and activation patterns of motor units. J Clin Neurophysiol 12:538-559.

Filipchuk AA, Durand J (2012) Postnatal dendritic development in lumbar motoneurons in mutant superoxide dismutase 1 mouse model of amyotrophic lateral sclerosis. Neuroscience 209:144-154.

Fleshman JW, Munson JB, Sypert GW, Friedman WA (1981) Rheobase, input resistance, and motor-unit type in medial gastrocnemius motoneurons in the cat. J Neurophysiol 46:1326-1338.

882 Foehring RC, Sypert GW, Munson JB (1987) Motor-unit properties following cross-reinnervation of
883 cat lateral gastrocnemius and soleus muscles with medial gastrocnemius nerve. II. influence of
884 muscle on motoneurons. J Neurophysiol 57:1227-1245.

885 Foehring RC, Sypert GW, Munson JB (1986) Properties of self-reinnervated motor units of medial
886 gastrocnemius of cat. II. axotomized motoneurons and time course of recovery. J Neurophysiol
887 55:947-965.

888 Fogarty, M. J.,Mu, E.W.H.,Lavidis, N.A.,Noakes, P.G.,Bellingham, M.C.(2020) Size-Dependent
889 vulnerability of lumbar motor neuron dendritic degeneration in SOD1 G93A mice. Anat. Rec., **303**,
890 1455.

891 Fogarty MJ, Omar TS, Zhan W, Mantilla CB, Sieck GC (2018) Phrenic motor neuron loss in aged rats.
892 J.Neurophysiol. 119:1852-1862.

893 Frank K, Fuortes M (1956) Stimulation of spinal motoneurones with intracellular electrodes.
894 J.Physiol.(Lond.) 134:451-470.

895 Friese A, Kaltschmidt JA, Ladle DR, Sigrist M, Jessell TM, Arber S (2009) Gamma and alpha motor
896 neurons distinguished by expression of transcription factor Err3. Proceedings of the National
897 Academy of Sciences - PNAS 106:13588-13593.

898 Fuglevand AJ, Macefield VG, Bigland-Ritchie B (1999) Force-frequency and fatigue properties of
899 motor units in muscles that control digits of the human hand. J Neurophysiol 81:1718-1729.

900 Gao H, Glatzer NR, Williams KW, Derbenev AV, Liu D, Smith BN (2009) Morphological and
901 electrophysiological features of motor neurons and putative interneurons in the dorsal vagal
902 complex of rats and mice. Brain research 1291:40-52.

903 Gardiner PF (1993) Physiological properties of motoneurons innervating different muscle unit types
904 in rat gastrocnemius. J Neurophysiol 69:1160-1170.

905 Garnett RAF, O'Donovan MJ, Stephens JA, Taylor A (1979) Motor unit organization of human medial
906 gastrocnemius. J. Physiol. 287:33-43.

907 Gentet L, Stuart GJ, Clements JD (2000) Direct measurement of specific membrane capacitance in
908 neurons. Biophys. J. 79:314-320.

909 Glenn LL, Dement WC (1981) Membrane resistance and rheobase of hindlimb motoneurons during
910 wakefulness and sleep. J Neurophysiol 46:1076-1088.

911 Goldberg LJ, Derfler B (1977) Relationship among recruitment order, spike amplitude, and twitch
912 tension of single motor units in human masseter muscle. J Neurophysiol 40:879-890.

913 Gustafsson, Pinter MJ (1985) On factors determining orderly recruitment of motor units: A role for
914 intrinsic membrane properties. Trends Neurosci. 431-433.

915 Gustafsson, Pinter MJ (1984a) Relations among passive electrical properties of lumbar alpha-
916 motoneurones of the cat. J. Physiol. 356:401-431.

Gustafsson, Pinter MJ (1984b) An investigation of threshold properties among cat spinal alpha-motoneurones. J. Physiol. 357:453-483.

Gustafsson B (1979) Changes in motoneurone electrical properties following axotomy. J. Physiol. 293:197-215.

Heckman CJ, Enoka RM (2012) Motor unit. Compr. Physiol. 2:2629-2682.

Hegedus J, Putman CT, Gordon T (2007) Time course of preferential motor unit loss in the SOD1 G93A mouse model of amyotrophic lateral sclerosis. Neurobiology of disease 28:154-164.

Henneman E (1985) The size-principle: A deterministic output emerges from a set of probabilistic connections. J. Exp. Biol. 115:105-112.

Henneman E (1981) Recruitment of motoneurons : The size principle. Motor Unit Types, Recruitment and Plasticity in Health and Disease 26-60.

Henneman E, Clamann HP, Gillies JD, Skinner RD (1974) Rank order of motoneurons within a pool: Law of combination. J Neurophysiol 37:1338-1349.

Henneman E, Somjen G, Carpenter DO (1965a) Functional significance of cell size in spinal motoneurons. J Neurophysiol 28:560-580.

Henneman E, Somjen G, Carpenter DO (1965b) Excitability and inhibitibility of motoneurons of different sizes. J Neurophysiol 28:599-620.

Henneman E (1957) Relation between size of neurons and their susceptibility to discharge. Science 126:1345-1347.

Highlander, M. M.,Allen, J.M.,Elbasiouny, S.M.(2020) Meta-analysis of biological variables' impact on spinal motoneuron electrophysiology data. Journal of Neurophysiology, **123**, 1380.

Huh, S.,Heckman, C.J.,Manuel, M.(2021) Time course of alterations in adult spinal motoneuron properties in the SOD1(G93A) mouse model of ALS. eNeuro, **8**, ENEURO.

Ishihara, A.,Kawano, F.,Ishioka, N.,Oishi, H.,Higashibata, A.,Shimazu, T.,Ohira, Y.(2001) Growth-related changes in cell body size and succinate dehydrogenase activity of spinal motoneurons innervating the rat soleus muscle. Int. j. dev. neurosci., **21**, 461.

Issa AN, Zhan W, Sieck GC, Mantilla CB (2010) Neuregulin-1 at synapses on phrenic motoneurons. J.Comp.Neurol. 518:4213-4225.

Izhikevich EM (2004) Which model to use for cortical spiking neurons? IEEE Trans.Neural Networks 15:1063-1070.

Jami L, Petit J (1975) Correlation between axonal conduction velocity and tetanic tension of motor units in four muscles of the cat hind limb. Brain Res. 96:114-118.

Kanda K, Hashizume K (1992) Factors causing difference in force output among motor units in the rat medial gastrocnemius muscle. J. Physiol. 448:677-695.

Kanjhan, R.,Fogarty, M.J.,Noakes, P.G.,Bellingham, M.C.(2015) Developmental changes in the morphology of mouse hypoglossal motor neurons. Brain Struct Funct, **221**, 3755.

Keen DA, Fuglevand AJ (2004) Distribution of motor unit force in human extensor digitorum assessed by spike-triggered averaging and intraneural microstimulation. J Neurophysiol 91:2515-2523.

Kernell D (2006) *The Motoneurone and its Muscle Fibres.* Oxford University Press UK, .

Kernell D, Zwaagstra B (1989) Dendrites of cat's spinal motoneurones: Relationship between stem diameter and predicted input conductance. J. Physiol. 413:255-269.

Kernell D, Monster AW (1981) Threshold current for repetitive impulse firing in motoneurones innervating muscle fibres of different fatigue sensitivity in the cat. Brain Res. 229:193-196.

Kernell D, Zwaagstra B (1981) Input conductance, axonal conduction velocity and cell size among hindlimb motoneurones of the cat. Brain Res. 204:311-326.

Kernell D (1966) Input resistance, electrical excitability, and size of ventral horn cells in cat spinal cord. Science 152:1637-1640.

Knott S, Lewis DM, Luck JC (1971) Motor unit areas in a cat limb muscle. Exp.Neurol. 30:475-483.

Krawitz S, Fedirchuk B, Dai Y, Jordan LM, McCrea DA (2001) State-dependent hyperpolarization of voltage threshold enhances motoneurone excitability during fictive locomotion in the cat. The Journal of physiology 532:271-281.

Krutki P, Hałuszka A, Mrówczyński W, Gardiner PF, Celichowski J (2015) Adaptations of motoneuron properties to chronic compensatory muscle overload. Journal of neurophysiology 113:2769-2777.

Lee RH, Heckman CJ (1998) Bistability in spinal motoneurons in vivo: Systematic variations in persistent inward currents. Journal of neurophysiology 80:583-593.

Li Y, Brewer D, Burke RE, Ascoli GA (2005) Developmental changes in spinal motoneuron dendrites in neonatal mice. Journal of comparative neurology (1911) 483:304-317.

Lucas SM, Ruff RL, Binder MD (1987) Specific tension measurements in single soleus and medial gastrocnemius muscle fibers of the cat. Exp.Neurol. 95:142-154.

Lux HD, Pollen DA (1966) Electrical constants of neurons in the motor cortex of the cat. J.Neurophysiol. 29:207-220.

Macefield VG, Fuglevand AJ, Bigland-Ritchie B (1996) Contractile properties of single motor units in human toe extensors assessed by intraneural motor axon stimulation. J Neurophysiol 75:2509-2519.

Major G, Larkman AU, Jonas P, Sakmann B, Jack JJ (1994) Detailed passive cable models of whole-cell recorded CA3 pyramidal neurons in rat hippocampal slices. J.Neurosci. 14:4613-4638.

Mantilla, C. B.,Zhan, W.,Gransee, H.M.,Prakash, Y.S.,Sieck, G.C.(2018) Phrenic motoneuron structural plasticity across models of diaphragm muscle paralysis. J Comp Neurol, **526**, 2973.

Manuel M, Chardon M, Tysseling V, Heckman CJ (2019) Scaling of motor output, from mouse to humans. Physiology (Bethesda, Md.) 34:5-13.

Manuel M, Heckman CJ (2011) Adult mouse motor units develop almost all of their force in the subprimary range: A new all-or-none strategy for force recruitment? Journal of Neuroscience 31:15188-15194.

Manuel M, Iglesias C, Donnet M, Leroy F, Heckman CJ, Zytnicki D (2009a) Fast kinetics, high-frequency oscillations, and subprimary firing range in adult mouse spinal motoneurons. The Journal of neuroscience 29:11246-11256.

Manuel M, Iglesias C, Donnet M, Leroy F, Heckman CJ, Zytnicki D (2009b) Fast kinetics, high-frequency oscillations, and subprimary firing range in adult mouse spinal motoneurons. The Journal of neuroscience 29:11246-11256.

Mateika JH, Essif EG, Dellorusso C, Fregosi RF (1998) Contractile properties of human nasal dilator motor units. J Neurophysiol 79:371-378.

McNulty PA, Macefield VG (2005) Intraneural microstimulation of motor axons in the study of human single motor units. Muscle & Nerve: Official Journal of the American Association of Electrodiagnostic Medicine 32:119-139.

McPhedran AM, Wuerker RB, Henneman E (1965) Properties of motor units in a homogeneous red muscle (soleus) of the cat. J Neurophysiol 28:71-84.

Mierzejewska-Krzyżowska B, Bukowska D, Taborowska M, Celichowski J (2014) Sex differences in the number and size of motoneurons innervating rat medial gastrocnemius muscle. Anatomia, histologia, embryologia 43:182-189.

Milner-Brown HS, Stein RB, Yemm R (1973) The orderly recruitment of human motor units during voluntary isometric contractions. J. Physiol. 230:359-370.

Mitra P, Brownstone RM (2012) An in vitro spinal cord slice preparation for recording from lumbar motoneurons of the adult mouse. Journal of Neurophysiology 107:728-741.

Moschovakis AK, Burke RE, Fyffe REW (1991) The size and dendritic structure of HRP-labeled gamma motoneurons in the cat spinal cord. Journal of comparative neurology (1911) 311:531-545.

Munson JB, Foehring RC, Lofton SA, Zengel JE, Sypert GW (1986) Plasticity of medial gastrocnemius motor units following cordotomy in the cat. Journal of neurophysiology 55:1454.

Nakanishi ST, Whelan PJ (2010) Diversification of intrinsic motoneuron electrical properties during normal development and botulinum Toxin–Induced muscle paralysis in early postnatal mice. J.Neurophysiol. 103:2833-2845.

Negro F, Yavuz U, Farina D (2016) The human motor neuron pools receive a dominant slow-varying common synaptic input. J. Physiol. 594:5491-5505.

Negro F, Yavuz U, Farina D (2014) Limitations of the spike-triggered averaging for estimating motor unit twitch force: A theoretical analysis. PloS one 9:e92390.

1020 Nordstrom MA, Miles TS (1990) Fatigue of single motor units in human masseter. J. Appl. Physiol.
1021 68:26-34.

1022 Obregón G, Ermilov LG, Wen-Zhi Z, Sieck GC, Mantilla CB (2009) Modeling dendritic arborization
1023 based on 3D-reconstructions of adult rat phrenic motoneurons. Revista Ingeniería Biomédica 3:47-
1024 54.

1025 Pinter MJ, Vanden Noven S (1989) Effects of preventing reinnervation on axotomized spinal
1026 motoneurons in the cat. I. motoneuron electrical properties. Journal of neurophysiology 62:311-324.

1027 Powers RK, Binder MD (2001) Input-output functions of mammalian motoneurons. Rev. Physiol.
1028 Biochem. Pharmacol. 143:137-263.

1029 Prakash YS, Mantilla CB, Zhan W, Smithson KG, Sieck GC (2000) Phrenic motoneuron morphology
1030 during rapid diaphragm muscle growth. Journal of Applied Physiology 89:563-572.

1031 Proske U, Waite PME (1974) Properties of types of motor units in the medial gastrocnemius muscle
1032 of the cat. Brain Res. 67:89-101.

1033 Rafuse VF, Pattullo MC, Gordon T (1997) Innervation ratio and motor unit force in large muscles: A
1034 study of chronically stimulated cat medial gastrocnemius. J. Physiol. 499:809-823.

1035 Rall W (1960) Membrane potential transients and membrane time constant of motoneurons.
1036 Exp.Neurol. 2:503-532.

1037 Rall W (1959) Branching dendritic trees and motoneuron membrane resistivity. Exp.Neurol. 1:491-
1038 527.

1039 Rall W (1957) Membrane time constant of motoneurons. Science 126:454.

1040 Reinking RM, Stephens JA, Stuart DG (1975) The motor units of cat medial gastrocnemius: Problem of
1041 their categorisation on the basis of mechanical properties. Exp. Brain Res. 23:301-313.

1042 Sasaki M (1991) Membrane properties of external urethral and external anal sphincter
1043 motoneurones in the cat. The Journal of physiology 440:345-366.

1044 Sica REP, McComas AJ (1971) Fast and slow twitch units in a human muscle. J. Neurol. Neurosurg.
1045 Psychiatry 34:113-120.

1046 Solsona C, Innocenti B, Fernández JM (1998) Regulation of exocytotic fusion by cell inflation.
1047 Biophys.J. 74:1061-1073.

1048 Song Z, Hu J, Rudy B, Redman SJ (2006) Developmental changes in the expression of calbindin and
1049 potassium-channel subunits Kv3. 1b and Kv3. 2 in mouse renshaw cells. Neuroscience 139:531-538.

1050 Spruston N, Johnston D (1992) Perforated patch-clamp analysis of the passive membrane properties
1051 of three classes of hippocampal neurons. J Neurophysiol 67:508-529.

1052 Stephens JA, Stuart DG (1975) The motor units of cat medial gastrocnemius: Speed-size relations and
1053 their significance for the recruitment order of motor units. Brain. Res. 91:177-195.

Stephens JA, Usherwood TP (1977) The mechanical properties of human motor units with special reference to their fatiguability and recruitment threshold. Brain Res. 125:91-97.

Sukhorukov VL, Arnold WM, Zimmermann U (1993) Hypotonically induced changes in the plasma membrane of cultured mammalian cells. J.Membr.Biol. 132:27-40.

Swett, Wikholm, Blanks, Conley (1986) Motoneurons of the rat sciatic nerve. Exp. Neurol. 93:227-252.

Taylor AM, Steege JW, Enoka RM (2002) Motor-unit synchronization alters spike-triggered average force in simulated contractions. J Neurophysiol 88:265-276.

Teeter C, Iyer R, Menon V, Gouwens N, Feng D, Berg J, Szafer A, Cain N, Zeng H, Hawrylycz M, Koch C, Mihalas S (2018) Generalized leaky integrate-and-fire models classify multiple neuron types. Nat Commun 9:1-15.

Thomas CK, Bigland-Richie B, Johansson RS (1991) Force-frequency relationships of human thenar motor units. J. Neurophysiol. 65:1509-1516.

Thomas CK, Johansson RS, Westling G, Bigland-Ritchie B (1990) Twitch properties of human thenar motor units measured in response to intraneural motor-axon stimulation. J Neurophysiol 64:1339-1346.

Thurbon D, Hans-R. Lüscher, Hofstetter T, Redman SJ (1998) Passive electrical properties of ventral horn neurons in rat spinal cord slices. J.Neurophysiol. 79:2485-2502.

Totosy de Zepetnek, Zung HV, Erdebil S, Gordon T (1992) Innervation ratio is an important determinant of force in normal and reinnervated rat tibialis anterior muscles. J Neurophysiol 67:1385-1403.

Turkin VV, O'Neill D, Jung R, Iarkov A, Hamm TM (2010) Characteristics and organization of discharge properties in rat hindlimb motoneurons. Journal of Neurophysiology 104:1549-1565.

Ulfhake, Kellerth JO (1981) A quantitative light microscopic study of the dendrites of cat spinal α-motoneurons after intracellular staining with horseradish peroxidase. J. Comp. Neurol. 202:571-583.

Ulfhake B, Kellerth JO (1984) Electrophysiological and morphological measurements in cat gastrocnemius and soleus α-motoneurones. Brain Res. 307:167-179.

Ulfhake B, Cullheim S (1988) Postnatal development of cat hind limb motoneurons. III: Changes in size of motoneurons supplying the triceps surae muscle. Journal of comparative neurology (1911) 278:103-120.

von Steyern FV, Martinov V, Rabben I, Njå A, de Lapeyrière O, Lømo T (1999) The homeodomain transcription factors islet 1 and HB9 are expressed in adult alpha and gamma motoneurons identified by selective retrograde tracing. The European journal of neuroscience 11:2093-2102.

Wuerker RB, McPhedran AM, Henneman E (1965) Properties of motor units in a heterogeneous pale muscle (m. gastrocnemius) of the cat. J.Neurophysiol. 28:85-99.

Yemm R (1977) The orderly recruitment of motor units of the masseter and temporal muscles during voluntary isometric contraction in man. J. Physiol. 265:163-174.

Young JL, Mayer RF (1982) Physiological alterations of motor units in hemiplegia. J. Neurol. Sci. 54:401-412.

Zengel JE, Reid SA, Sypert GW, Munson JB (1985) Membrane electrical properties and prediction of motor-unit type of medial gastrocnemius motoneurons in the cat. J Neurophysiol 53:1323-1344.

Zwaagstra, Kernell (1981) Sizes of soma and stem dendrites in intracellularly labelled α-motoneurones of the cat. Brain Research 204:295-309.

Zwaagstra B, Kernell D (1980) The duration of after-hyperpolarization in hindlimb alpha motoneurones of different sizes in the cat. Neurosci. Lett. 19:303-307.